AD-751 134

THE DESIGN AND ANALYSIS OF A HUMAN BODY MOTION MEASUREMENT SYSTEM

L. Jack Little

Army Missile Command
Redstone Arsenal, Alabama

September 1972

UNCLASSIFIED
Security Classification

DOCUMENT CONTROL DATA - R & D

(Security classification of title, body of abstract and indexing annotation must be entered when the overall report is classified)

1. ORIGINATING ACTIVITY (Corporate author)
Guidance and Control Directorate
Directorate for kes, Dev, Eng & Msl Sys Lab
US Army Missile Command
Redstone Arsenal, Alabama 35809

2a. REPORT SECURITY CLASSIFICATION
UNCLASSIFIED

2b. GROUP
NA

3. REPORT TITLE

THE DESIGN AND ANALYSIS OF A HUMAN BODY MOTION MEASUREMENT SYSTEM

4. DESCRIPTIVE NOTES (Type of report and inclusive dates)
Technical Report

5. AUTHOR(S) (First name, middle initial, last name)

L. Jack Little

6. REPORT DATE	7a. TOTAL NO. OF PAGES	7b. NO. OF REFS
September 1972	90	8

8a. CONTRACT OR GRANT NO.	9a. ORIGINATOR'S REPORT NUMBER(S)
b. PROJECT NO. (DA) 1X222251D231	Technical Report RG-72-19
c. AMC Management Structure Code No. 527E.12.12500	9b. OTHER REPORT NO(S) (Any other numbers that may be assigned this report)
d.	AD_____

10. DISTRIBUTION STATEMENT

Approved for public release; distribution unlimited.

11. SUPPLEMENTARY NOTES	12. SPONSORING MILITARY ACTIVITY
None.	Same as No. 1

13. ABSTRACT

No adequate systems were found in a literature search that would permit direct measurement of human body segments' angular acceleration and muscle forces related to these accelerations which would allow application of analytic mechanics to the human motion problem. Therefore, a new system was designed and analyzed to provide accurate measurement of the body segments' motion directly by use of angular accelcrometers.

The basic elements of the system are the accelerometers, all electromyogram sensors, and a proportional bandwidth telemetry system that allows the human performer to move about freely.

Verification of the system was accomplished by measurement of angular accelerations of the arm and leg links during kip-up maneuvers. Alignment of the accelerometers was achieved by an optical laser technique. The acceleration signals, stored on magnetic tape, were subsequently integrated to get rate and position in an inertial reference frame. These position data, obtained through integration, proved to be sufficiently accurate when compared with synchronized position data obtained from high speed motion picture film data.

DD FORM 1 NOV 65 1473 REPLACES DD FORM 1473, 1 JAN 64, WHICH IS OBSOLETE FOR ARMY USE.

UNCLASSIFIED
Security Classification

14. KEY WORDS	LINK A		LINK B		LINK C	
	ROLE	WT	ROLE	WT	ROLE	WT
Human body segments' angular acceleration Measurement of body segments' motion Electromyogram sensors Optical laser technique						

AD

TECHNICAL REPORT
RG-72-19

THE DESIGN AND ANALYSIS OF A HUMAN BODY MOTION MEASUREMENT SYSTEM

by

L. Jack Little

September 1972

Approved for public release; distribution unlimited.

U.S. ARMY MISSILE COMMAND
Redstone Arsenal, Alabama

93

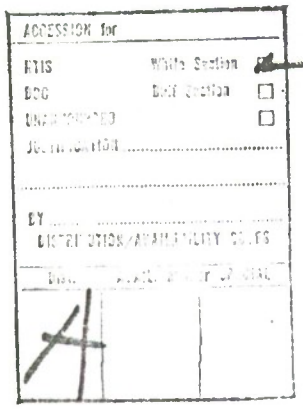

DISPOSITION INSTRUCTIONS

DESTROY THIS REPORT WHEN IT IS NO LONGER NEEDED. DO NOT RETURN IT TO THE ORIGINATOR.

DISCLAIMER

THE FINDINGS IN THIS REPORT ARE NOT TO BE CONSTRUED AS AN OFFICIAL DEPARTMENT OF THE ARMY POSITION UNLESS SO DESIGNATED BY OTHER AUTHORIZED DOCUMENTS.

TRADE NAMES

USE OF TRADE NAMES OR MANUFACTURERS IN THIS REPORT DOES NOT CONSTITUTE AN OFFICIAL INDORSEMENT OR APPROVAL OF THE USE OF SUCH COMMERCIAL HARDWARE OR SOFTWARE.

September 1972

Technical Report RG-72-19

THE DESIGN AND ANALYSIS OF A HUMAN BODY MOTION MEASUREMENT SYSTEM

by

L. Jack Little

DA Project No. 1X222251D231
AMC Management Structure Code No. 527E.12.12500

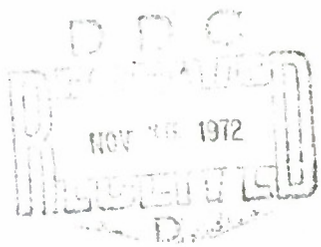

Approved for public release; distribution unlimited.

Guidance and Control Directorate
Directorate for Research, Development, Engineering
and Missile Systems Laboratory
US Army Missile Command
Redstone Arsenal, Alabama 35809

ABSTRACT

No adequate systems were found in a literature search that would permit direct measurement of human body segments' angular acceleration and muscle forces related to these accelerations which would allow application of analytic mechanics to the human motion problem. Therefore, a new system was designed and analyzed to provide accurate measurement of the body segments' motion directly by use of angular accelerometers.

The basic elements of the system are the accelerometers, all electromyogram sensors, and a proportional bandwidth telemetry system that allows the human performer to move about freely.

Verification of the system was accomplished by measurement of angular accelerations of the arm and leg links during kip-up maneuvers. Alignment of the accelerometers was achieved by an optical laser technique. The acceleration signals, stored on magnetic tape, were subsequently integrated to get rate and position in an inertial reference frame. These position data, obtained through integration, proved to be sufficiently accurate when compared with synchronized position data obtained from high speed motion picture film data.

TABLE OF CONTENTS

CHAPTER I. INTRODUCTION

Motivation

It is the goal of this effort to develop instrumentation and a scientific procedure that will enable collecting empirical data to comprehensively analyze the human body motions and inherent forces from which an optimal mathematical model may be generated. This thesis proposes employing an angular accelerometer to measure the acceleration of the various body elements and transmitting this information by telemetry to a remote data processing point such that on-line data evaluation can be accomplished. The optimal model is not the goal here. The present emphasis is to establish feasibility of the method not to arrive at the optimal model.

Earlier research associated with body motion utilized motion picture film to obtain position data of the various body elements. This source of data is inherently noisy and has a significant variance. Differentiation of these noisy data is required to obtain the necessary rate and acceleration information for modeling the human motion. Integration of noisy data results in an improvement in the processed data. Thus we should gather raw data that require only integration. This, in theory, can be accomplished by measuring the highest derivative and integrating. Because the highest derivative required is that corresponding to angular acceleration, it is natural to obtain the raw data from an angular accelerometer. These data can then be integrated to obtain accurate rate and position information.

The ability to automate the data processing through the application of the angular accelerometer reduces the human errors and decreases the manhours expended in data analysis of the motion picture film.

Earlier research efforts, relevant to body motion that were reviewed, failed to correlate body motion and the muscle forces that generated the forcing function necessary to cause the body motion. Hence, an apparent question that must be answered before modeling body motion can be accomplished would be, what force magnitude generated by what muscle group is manifested in producing a given acceleration? By inclusion of electromyogram (EMG) sensors, monitoring strategic muscle groups, these data can be supplied simultaneously with the acceleration data thus enabling correlation of body motion and the associated forces.

Previous Related Research

Literature Search

The Defense Documentation Center (DDC) and the NASA Document Center (STAR) were employed through a computer search for documents related to human body motion studies and the instrumentation of such studies. No time limit was placed on the documents origin and a security classification through secret was requested. A broad spectrum of descriptors was used to insure retrieving any document remotely related to the subject of the search. Various combinations of the descriptors were used to give a thorough search. The hierarchy of descriptors used in this search produced approximately 800 titles. Of these 800 titles, only 30 of the abstracts proved to be even remotely related to the subject.

Related Research

The dynamics of the human body have intrigued the scientific community for a number of years. The efforts were, in essence, directed toward a particular facet such as the variation of strength during body movement. N. T. V. Geneesk [1] performed research in 1921 that was associated with forces in body motion. This research proved relevant to NASA's space program and apparently contained valid information concerning muscle strength. Because the end result of this thesis is to develop equipment and an experiment that will enable collecting data for an optimal model of the human body motions, it would be noteworthy to make some comments concerning Geneesk's results. In the experiments reported, it was found that the muscle forces build up rather sharply from age six to approximately age 22. At the latter age, a gradual decline in muscle forces are experienced up to age 60. These measurements were made from a good statistical cross section of male and female subjects. Also, the strength of women, observed from these data, tended to be approximately 60 percent that of the male throughout the time span.

Another significant factor was the absolute strength figure of 5.6 kg/cm^2 for the muscle where this is related to the cross-sectional area of the muscle. This would be useful as a scale factor in physiometric data of a given subject relative to a generalized model.

As time progressed, computers began to play a part in the study of human motions. N. Eshkol et al. [2] reported the development of a computer program that assembled the human motion in a system of links representing various joints and parts of the human body. However, this

program merely produces the motions of the various parts of the body by virtue of and within geometric boundaries such as cones, spheres, planes, etc. Hence such kinematical study, by way of a cathode ray display, enables the analysis of the motion capabilities of the human body.

Similarly, H. Calvity et al. [3] reported developing a differential equation model of the human body using a Lagrangian approach with the ability to introduce specific forcing functions as an input to the human system model. The object was to observe the effects of loads on the human body due to loads such as that incurred when firing an M-1 rifle. Again the computer was utilized in the analysis. The human body system was modeled from static measurements and the dynamics were generated by the computer. No measured dynamic data or system of collecting the data was evident in this study. J. Ramsey et al. [4, 5] performed experiments in human body motion through the application of a stereoscopic photographic technique. This approach has apparent limitations and inherent inaccuracies because of the inability to maintain a fixed reference frame. In those few documents related to human body motion studies, no dynamic data were presented that would lend itself to modeling techniques. Most of the related efforts dealt with specific functions or movements associated with performing a simple task.

The lack of information in regard to the instrumenting of the human body for motion studies was more evident. E. Edwards [6] detailed an experiment where two piezo-crystal accelerometers were attached to the hand of a subject and the subject performed a simple tapping motion

with a hammer. The motion was maintained in a vertical plane. A erations and velocities were measured during the experiment. How the measurements at most were qualitative because of the constant changing direction of the local gravity vector as the accelerometer moved in the vertical plane.

W. Hixson et al. [7] described a biotelemetry system for stud of humans under zero g conditions. The experiment performed by the Hixson team required suspending a subject in a zero g environment a measuring the physiological parameters of the subject. The zero g environment was generated by flying a KC-135 jet aircraft through a ballistic profile. The subject was strapped to a platform instrumen with accelerometers and biomedical sensors. The data from these instruments were telemetered to an on-board telemetry receiver syste where the data were demodulated and stored on strip chart recordings. The biomedical sensors used in this experiment produce signal levels much lower in amplitude than those of the EMG sensors employed in the current research. Also, the signals were periodic. Secondly, the inertial sensors used in this experiment were measuring the inertial stability of the platform motion rather than a broad range of motion that is expected in the current research. There are similarities between the instrument system described by Hixson and the one developed by the author. Both systems employ a proportional bandwidth subcarrier type frequency modulation and variable frequency oscillators as analog to frequency converters. However, the signal bandwidth and signal dynamics of the current system will be more demanding than those of the system described by Hixson.

Summary of Related Research

Earlier research in the area of measuring body motion and forces incurred during the motion have not comprehensively exhibited the optimal capabilities of the man machine.

A variation of the telemetry system described by W. Hixson [7] will be used in this research although the idea was conceived before reviewing the report. Hixson's efforts were concerned with measuring respiration under a fixed inertial environment whereby most of his signal levels were relatively small. The parameters in this research are the measurement of motion in an inertial reference frame and the forces generating these motions. However, it is advantageous to use telemetry in extracting data from the isolated test environment to avoid extraneous signals and to free the movement of the test subject.

The works of Geneesk [1] imply that a figure of force can be extracted from the motion and measurement on the muscles. Dynamometer measurements in conjunction with EMG measurements produced sufficient evidence that EMG sensors can be used as a dynamic measure of muscle forces and these sensors can be applied to study forces for any motion. Hence EMG signals will be used as a measure of muscle forces generated during the body motion.

In view of the limited work of N. Eshkol et al. [2] and H. Calvity et al. [3] in the development of models from static measurements, their only concern was with ranges of motions and the responses or loads imposed on the body as the result of various forcing functions.

The related research reviewed was not concerned with dynamic body motions as applied to optimal modeling. Now techniques are developed that will enable collecting accurate data such that an optimal model of the man machine can be realized.

Present Researeh

Human Motion Model

The rigid body model of human motion used in this study is for a subject performing a kip-up while suspended on a parallel bar. The human motion model is simplified to a three-link system, and three angles have been defined to describe the relative motion of the three-link system (Figure 1). The forcing function that induees this motion is described in terms of replacement of musele forees or the changing angle (ψ) between the leg segment and the torso segment and angular deviation (θ) between the arm segment and the torso. A third angle (φ), the angle between arm segment and a reference line that is perpendicular to the parallel bar, is the depende t variable and a generalized coordinate. These angles are easily established in a reference frame for the photographic portion of the experiment. However, a transformation was used to establish the absolute angles between the three body links and an inertial reference frame. Hence, $\mu = \varphi$, $\alpha = \mu - \theta$, and $\nu = \alpha - \psi$ will describe the angles in the inertial frame and allow correlation between the inertial frame angles and the relative angles of the model.

For use in the equations of motion it will be neeessary to measure the acceleration, velocity, and displacement of the relative three angles. Figure 2 illustrates the model of the three-link system and the relation between the two reference frames.

The forcing funetion producing the motion previously deseribed is generated by voluntary musele forees in the thighs, hips, shoulders,

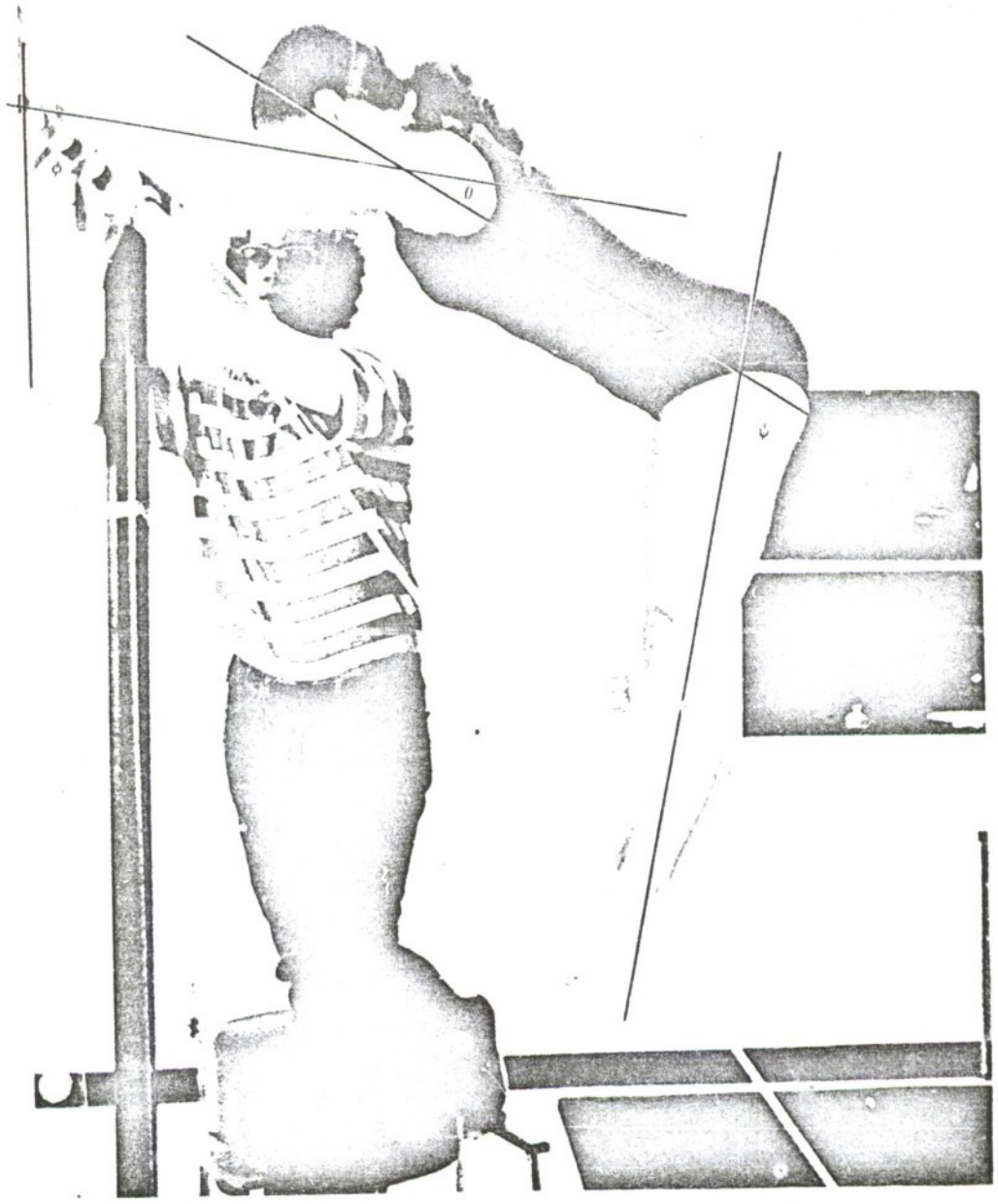

Figure 1. Bar reference frame

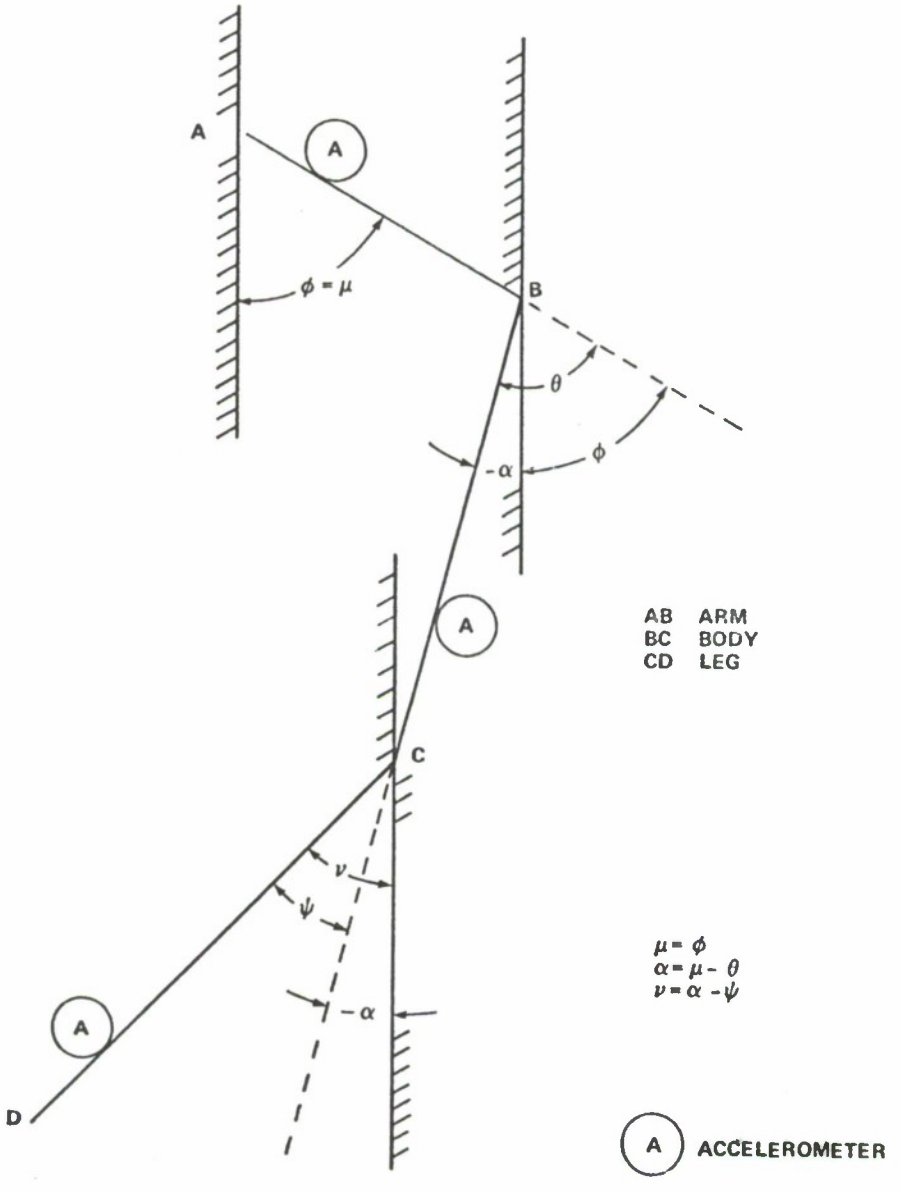

Figure 2. Reference frame transformation and sensor location

and arms. These forces will be measured by electromyography. In the optimization process, these six muscle force parameters will be employed in producing a figure of work. It should be noted that those measurements specified are not the only ones possible. Any portion of the

body that moves as a nearly rigid body in the inertial referenee frame and has adequate space to mount a sensor ean be instrumented for rigid body motion.

Feasibility

During the feasibility phase, the goal of this thesis, a single angular accelerometer and one set of EMG electrodes were used to prove the validity of the coneept set forth. Future researeh will use a minimum of six angular aecelerometers and six sets of EMG electrodes. Figure 2 illustrates the potential aeeelerometer and EMG mounting positions necessary to collect the basie data already deseribed. These mounting points are tentative and future experimenters will have the flexibility to position the sensors at will.

As previously mentioned, the single angular aceelerometer will be mounted on the forearm and the EMG eleetrodes will be attached to the upper arm museles.

By judieious placement of the accelerometers, the angular acceleration of any segment of the body ean be measured. The angular accelerometer measures the angular acceleration of a particular body segment and these data are telemetered out of the test subjects environment over a single data channel. Through data processing off board, two additional parameters can be realized: the angular rate (e.g., $\dot{\phi}$) and the angular displacement (e.g., ϕ) of a given body link. These are obtained by integration of the telemetered signal. In summary, the instrumentation system will be eomprised of EMG sensors, angular accelerometers, telemetry, and analog eomputer. Figure 3 illustrates diagrammatically the flow of data.

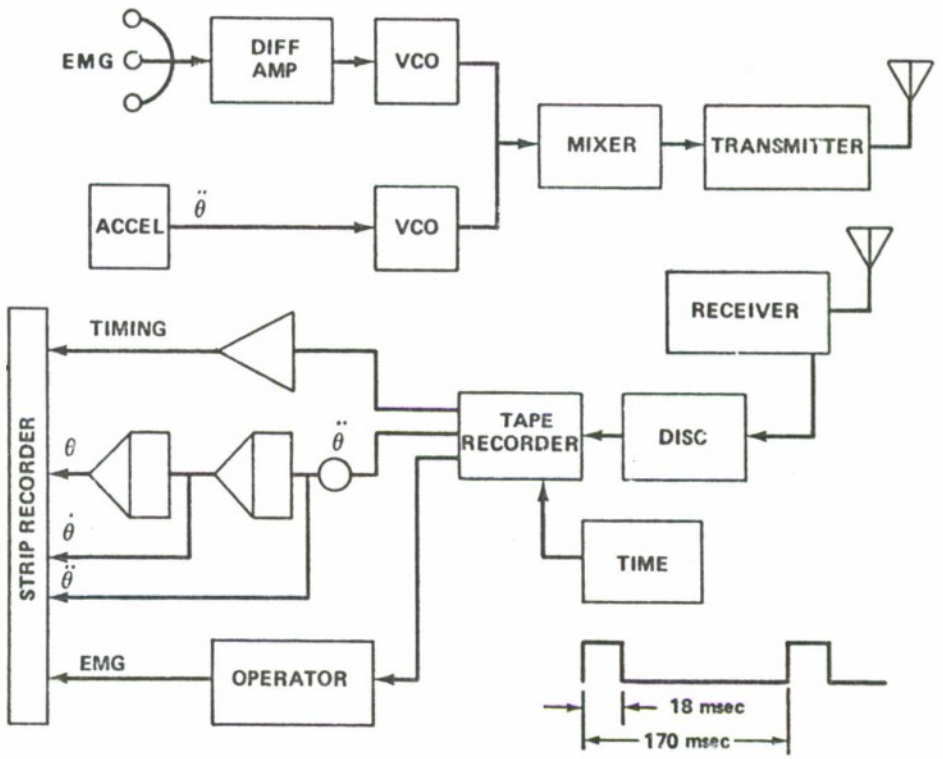

Figure 3. System data flow

This particular approach is advantageous because 24 pieces of data can be collected through six telemetry channels. This is achieved without encumbering the test subject with a maze of wires connecting him to the outside world. Naturally, there will be leads from the 12 various sensors; however, these may be placed in contact with the skin surface without impairing the subjects motion. The sensor leads, the telemetry package that is mounted on the subjects lower back, and the sensors will be the total external influence of the test environment. The total weight of the system mounted on the test subject is approximately 3 kg.

By using a telemetry system as a means of collecting data, the data may be relayed directly to a remote computer site such that real

time data manipulations can be realized. This inherently provides a means to store the data in a variety of formats.

The systems approach to collecting body motion data is certainly a step forward in mechanizing and improving the accuracy of the data when compared to earlier endeavors. For example, this approach proves to be quite advantageous over the photographic technique. The data are subject to errors and therefore result in large errors in angular speed and angular acceleration obtained by differentiating the noisy data. Also, the photographic technique required analyzing each frame to determine the motion and depended on accurate frame rates to determine the angular rates. The large number of measurements required and calculations consume many valuable manhours. In addition to the saving in manhours, this relatively sophisticated system is estimated to be at least an order of magnitude more accurate than other techniques employed in body motion studies. The accuracy of the system can be demonstrated by inspecting the component errors and assimilating the component errors in a conventional statistical format such that a figure of merit may be realized for the entire system. A theoretical analysis was performed and compared with empirical data justifying the feasibility of the angular accelerometer system and its accuracy. There are conceivably four mechanizations to achieve the goals set forth in this thesis:

a) Use of linear accelerometers for the motion measurements is impractical because the local gravity vector would produce an input to the accelerometers as the relative position of the accelerometer sensitive axis to the g vector varied with movement. This would entail a very complex system just to remove the effects of the local gravity.

b) Build a mechanical linkage with position sensors at each joint such that the desired motions could be monitored by the sensor at each link. This is possible but not very practical because the subject's motion would be hindered by a maze of wires and linkages and the data would still require differentiation.

c) The problems with the photographic technique have been mentioned.

d) Use of angular accelerometers have none of the shortcomings of the other methods, if the accelerometers have adequate dynamic range.

Conceivably, the application of angular accelerometers, EMG sensors, and telemetry data links should provide a system capable of measuring the human body motion with an overall system inaccuracy of about 2 percent.

CHAPTER II. SYSTEM DESIGN

Accelerometer

Instrument Description

Inertial sensors are a means of detecting body motions in an isolated environment. The angular accelerometer was selected because measurements of angular acceleration and rate parameters of the various links in the body system are required without the effects of local gravity and the position of the detecting instrument on the link.

A Systron Donner model 4591 fluid rotor angular accelerometer (Figure 4) was selected because of its size and dynamic range characteristics. Essentially, the device consists of a toroid filled with a fluid that acts as a seismic mass. Flow of this fluid with respect to the toroid or case provides a means of detecting the inertial forces on the device. A servoed paddle is placed in the flow of the fluid hence physically blocking the flow of the fluid. Therefore, the effort expended in holding the paddle fixed, by servo action, against the flow of fluid is a direct measure of the inertial reaction force on the paddle due to the acceleration. The fluid toroid (Figure 5) is in a plane normal to the sensitive axis and the paddle axis of rotation is colinear with the sensitive axis. The sensor is diagramatically shown in Figure 6. When the toroid is accelerated in a positive sense, as denoted by arrow 1 of Figure 6, the fluid produces a net force on the paddle at 2. The force at point 2 causes a displacement in the pickoff that in turn

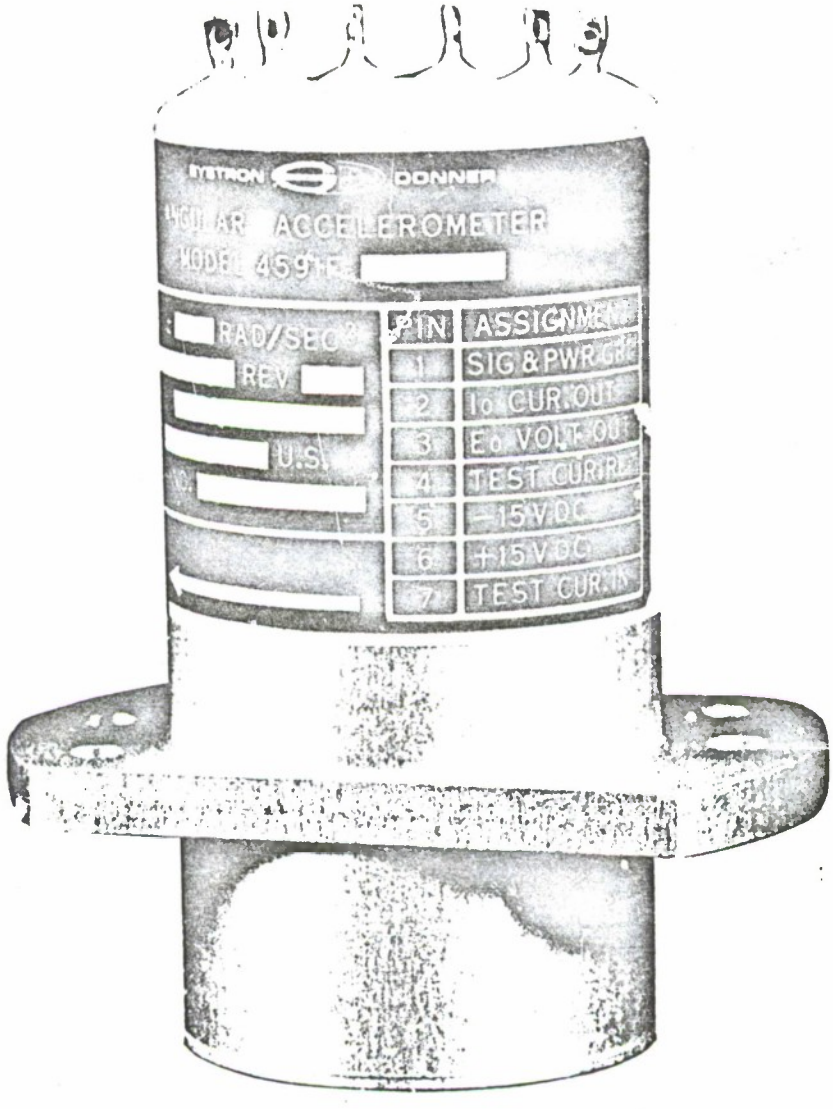

Figure 4. Model 4591 fluid rotor angular accelerometer

produces an error signal at the input to the amplifier. The output of the amplifier is fed into the torque coil which serves to drive the paddle back to the null position relative to the case and pickoff. The force generated by the torque coil acts to hold the paddle fixed relative to the accelerometer case. Hence the current necessary to

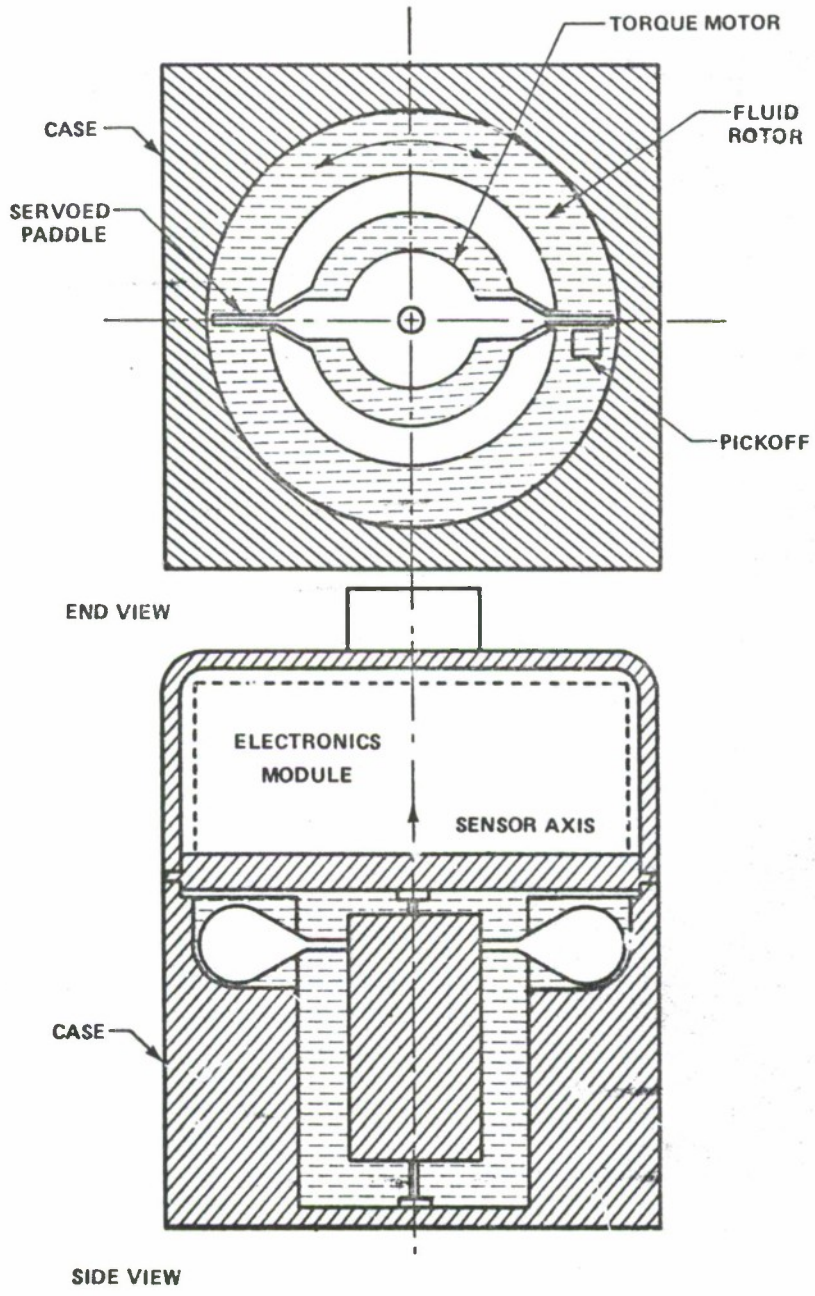

Figure 5. Fluid rotor and paddle mechanism

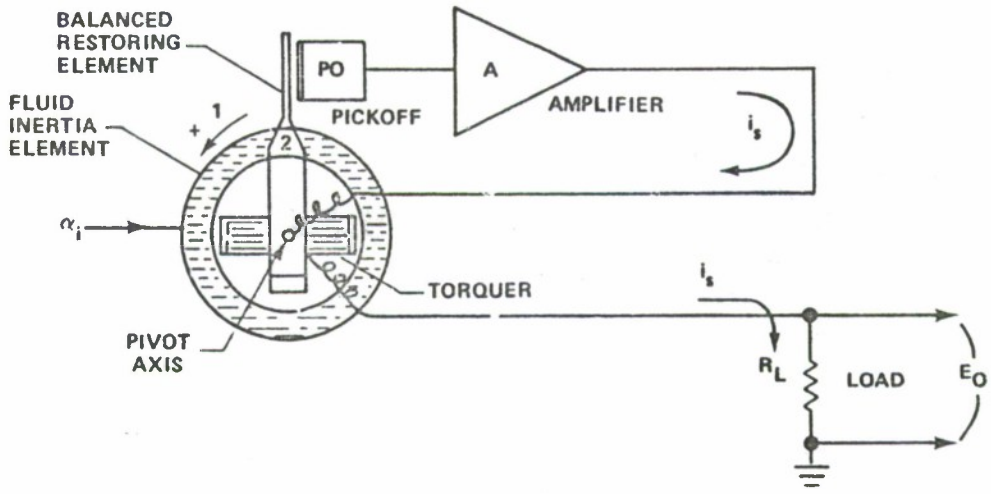

Figure 6. Basic block diagram of the fluid rotor angular accelerometer

hold the paddle fixed against the fluid flow is proportional to the force produced to accelerate the fluid or proportional to the angular acceleration.

The transfer function of the mechanical and electrical components of the accelerometer is

$$\frac{e_o}{a_i} = \frac{K_a \omega_n^2}{s^2 + 2\zeta\omega_n s + \omega_n^2}$$

The system can be assumed to be a second-order low pass filter. The gain factor (K_a) of scale factor produces an output voltage across the resistor R_L proportional to the angular acceleration.

Instrument Selection Criterion

Due to the wide dynamic range of the body motion experiment and the inability to establish an absolutely rigid reference for the system, some compromises were required to obtain a cost effective

system of sufficient accuracy. Some misalignment of the accelerometer with respect to its pivot axis will occur. A sacrifice in hysteresis and resolution must be made to obtain the desired dynamic range from the accelerometer. The inability to quite rigidly position the accelerometer in its reference frame is accepted for reduced weight and constraints on the subject. For a thorough error analysis over extreme ranges of motion, sets of measurements were selected that would be most representative.

It was concluded from previous* film data of the wide dynamic range kip-up motion that the arm link and the leg link of the body system would be most descriptive in mounting errors and extreme ranges of acceleration and position inputs. These mounting positions would also allow evaluation of alignment procedures for the accelerometer.

A bracket was made to maintain the alignment of an arm link accelerometer within 1 degree of arc during arm link measurements. This required no special alignment procedures. However, the gimbal bracket to mount the accelerometer to the leg should hold the alignment only within 4 degrees of arc. The initial alignment for the leg mount was accomplished with a laser to within 1 degree of arc.

During this feasibility study, only one accelerometer was used. The single accelerometer was rigidly attached to a bracket that had simple rotation about the high bar (Figure 7). The bracket with the accelerometer is strapped to the subjects forearm to couple the angular acceleration of the subject to the accelerometer and still maintain

*This work was performed by T. K. Ghosh, a Ph.D. candidate in Engineering Science and Mechanics, and Dr. Boykin (to be published).

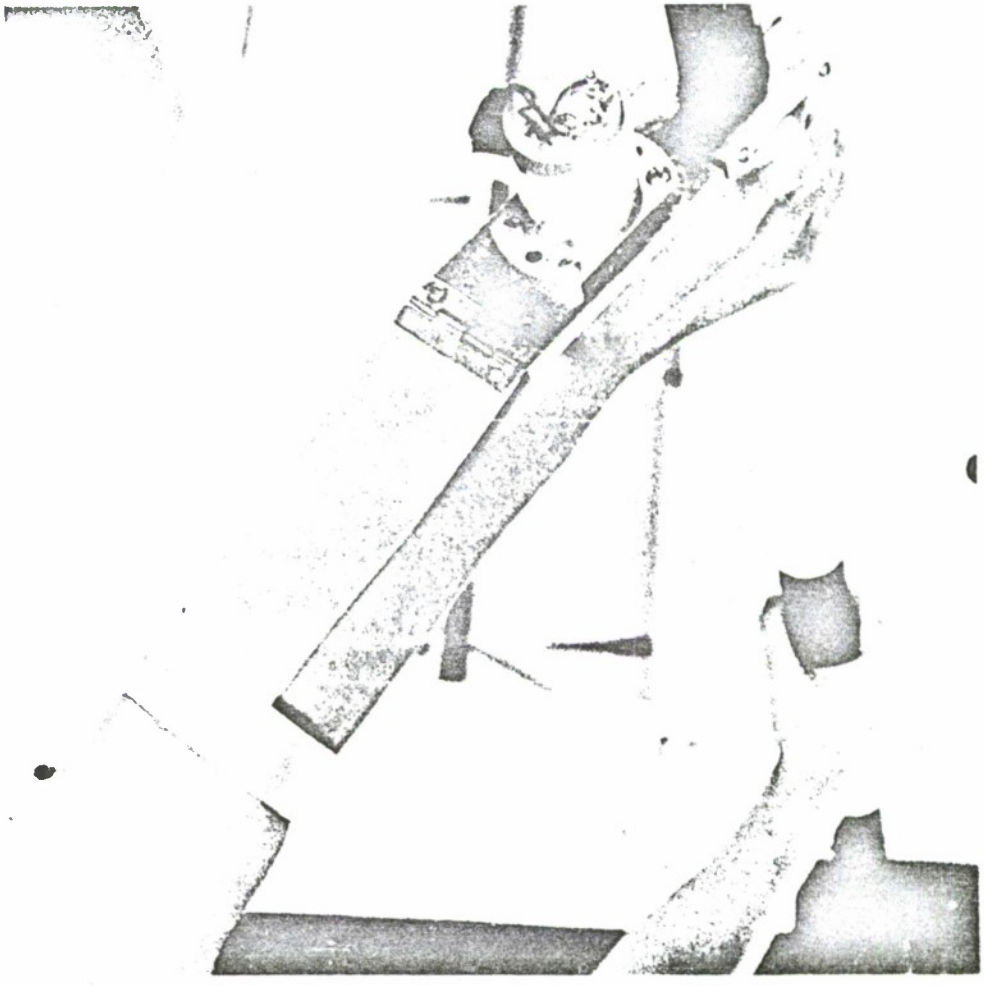

Figure 7. High bar and arm bracket mounting

alignment accuracy. This mount for a single accelerometer allows mounting the accelerometer to within 1 degree of arc and maintains this alignment. Because of the potential misalignment errors in other link mounts, the cross axis coupling and sensitivity to linear acceleration were considered in the selection of an accelerometer.

The dynamic range of the accelerometer was selected from data collected earlier by photographic techniques (Figure 8). During this earlier study, body accelerations and rates were determined from sequential body positions in a series of pictures filmed at 60 frames per second. From the data, it was determined that the lowest acceleration would be 0.01 rad/sec-sec and the maximum acceleration would be less than 150 rad/sec-sec. Hence, an accelerometer with a resolution of 0.01 rad/sec^2 and a maximum dynamic range of 200 rad/sec^2 was considered suitable for the required measurements. A 50 rad/sec^2 accelerometer was available, but for this feasibility study the 200 rad/sec^2 accelerometer was chosen to insure sufficient range and avoid saturation.

Since the maximum range of the accelerometer is predicated on earlier data, only the scale factor for the accelerometer needs to be specified. Since the available variable frequency oscillators that will be used for the analog to frequency conversion have a ± 2.5-Vdc input range, the accelerometer scale factor will be selected accordingly. Thus,

$$\text{Scale Factor (SF)} = \frac{2.5 \text{ volts}}{200 \text{ rad/sec}^2}$$

or a 12.5-mV/rad/sec^2 scale factor will nearly utilize the full dynamic range of the variable frequency oscillators (VCO).

Threshold, resolution, and linearity are all predicated on the instruments hysteresis curve. This is discussed in the error analysis section. For the body motion experiment, it was necessary to hold a

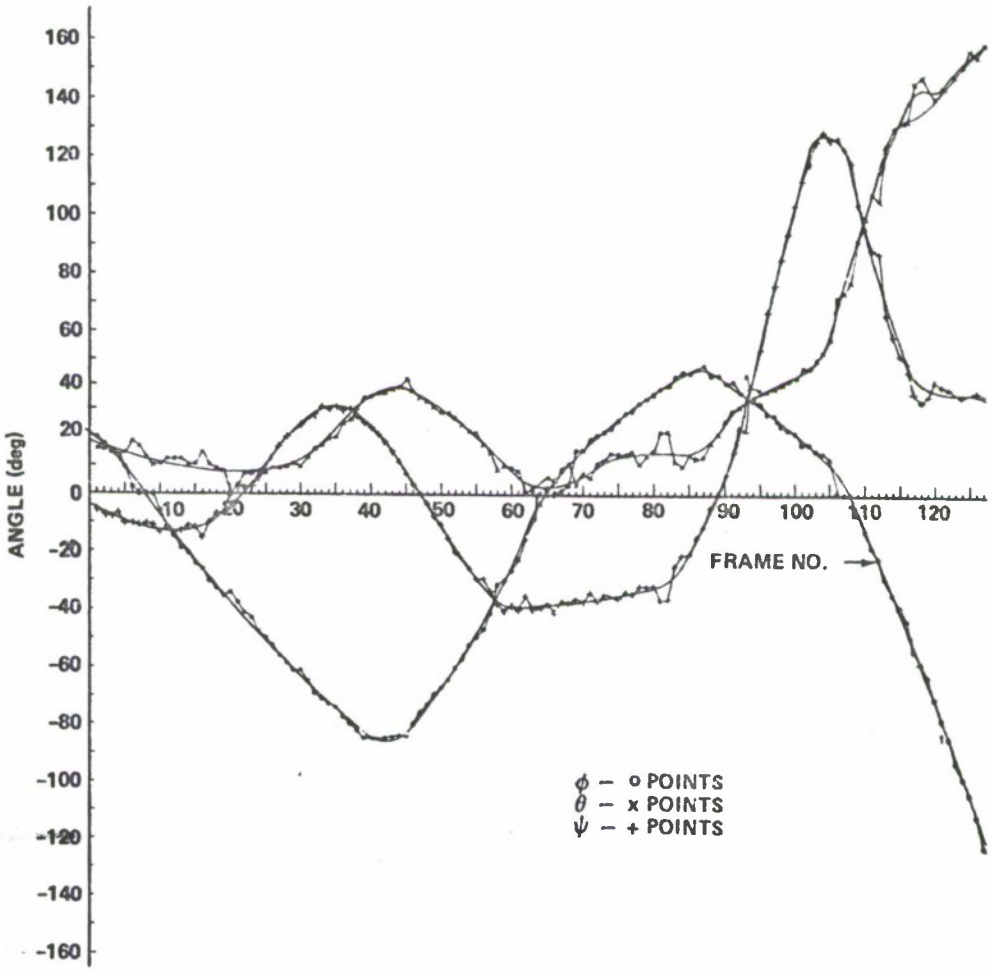

Figure 8. Body motions of the three link system from pictorial data

tight tolerance on hysteresis because of the subsequent integrations necessary to obtain the rate and positions data. Angular rate and angular displacement were extracted from the acceleration signal by integration on an analog computer, hence any offset resulted in errors that increase with time.

These requirements were given foremost consideration in the selection of an inertial instrument along with secondary parameters

such as noise, size, temperature coefficient, and power requirements. The latter parameters are commonly state-of-the-art specifications that can be readily obtained. These data led to selecting the Systron Donner model 4591 angular accelerometer.

Error Analysis

The ideal accelerometer will have a linear input/output relationship as depicted in Figure 9; however, because we must operate in the real world where nothing is ideal, one must make concessions. Such is the case with an accelerometer. The fluid rotor accelerometer has imperfections just as any other mechanical device. The model 4591 has a conventional second-order transfer function:

$$\frac{e_o}{a_i} = \frac{K_a \omega_n^2}{s^2 + 2\zeta\omega_n s + \omega_n^2}$$

where ω_n = 111 Hz, ζ = 0.69, and K_a = 0.0204 volts/rad/sec^2. Because the instrument operated in a reasonably constant environment, the temperature coefficient of 0.03 percent of the voltage scale factor does not contribute a significant error. Hence the parameters of the accelerometer affected by temperature, namely damping and natural frequency, will remain essentially constant. However, the paramount errors are associated with the scale factor, its hysteresis and linearity, and the mechanical attributes such as stiction and pivot-jewel friction. Table I contains the vendors pertinent specifications to be used in the error analysis for the accelerometer.

The hysteresis and resolution error presents a composite picture of the dynamics performance for the accelerometer. This is illustrated graphically by Figures 10 and 11. Line segment AOB of Figure 10

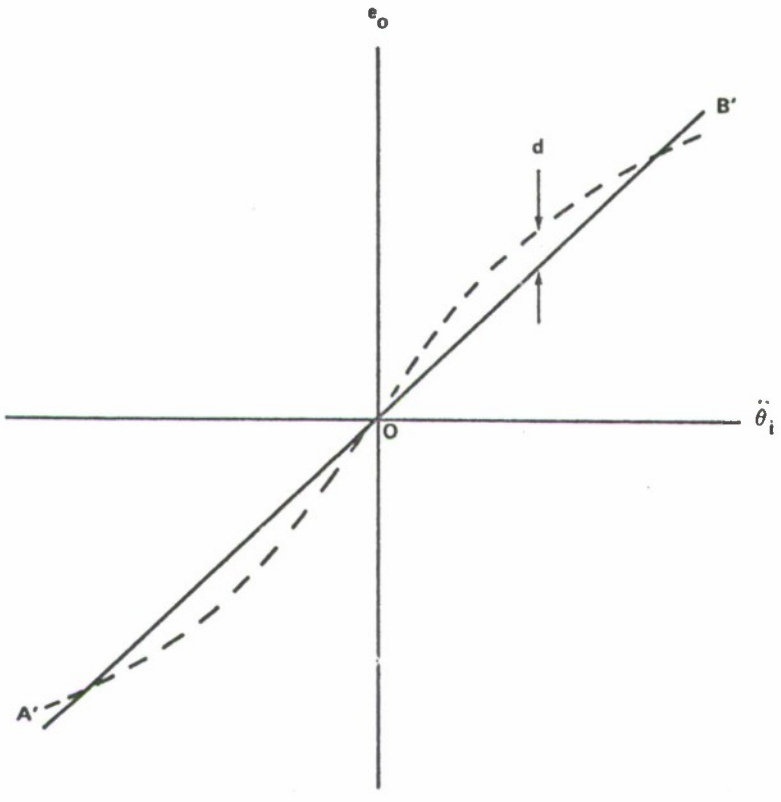

Figure 9. Accelerometer input/output curve

represents the ideal straight line scale factor which is tangent to the nonlinear characteristic at O. Line segment A'OB' represents the actual scale factor which is a best fit line to the nonlinear characteristic over full scale. Thus, an approximation to the ideal scale factor is realized by using a best fitted straight line between points A', O, and B'.

Employing this approximation, one can define a maximum nonlinearity discrepancy of amplitude d as shown in Figures 9 and 11. By using the given nonlinearity figure of 0.1 percent, it can be

Table I. Accelerometer specifications

K_a Scale Factor	0.0204 volts/rad/sec^2
Hysteresis and Resolution	0.05 percent full scale
Noise	2.5 mV rms
Bias	0.0002 Vdc
Cross Axis Sensitivity	3 mV/rad/sec^2 (maximum)
Linear Acceleration Sensitivity	0.9 mV/g
Nonrepeatibility	0.02 percent full scale
Temperature Sensitivity:	
Scale Factor	0.0242 percent/°F
Bias	0.00625 mV/°F
Nonlinearity	0.1 percent full scale

shown that the value for d is,

$$d = \text{percent nonlinearity} \times \text{full scale input}$$

$$d = 1 \times 10^{-3} \times 2 \times 10^{2} \text{ rad/sec}^2$$

$$d = 0.2 \text{ rad/sec}^2 = 11.46 \text{ deg/sec}^2$$

which is a constant term with respect to time. The entire scale factor slope can shift because of the effects of the temperature, but the nonlinearity characteristics remain essentially the same. The scale factor slope changes can be as great as 0.024 percent/°F which is negligible when the ambient temperature change over a test interval is less than 1°F. For example,

$$\Delta SF = SF \times 1°F \times \text{temperature sensitivity}$$

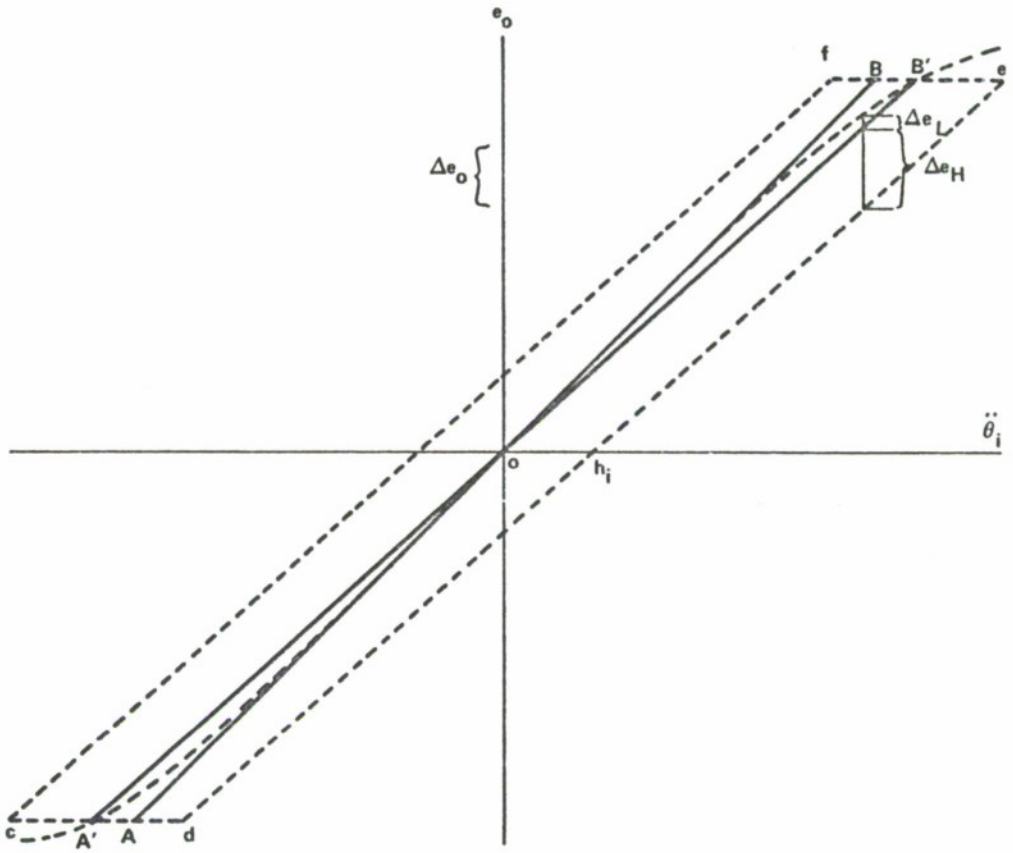

Figure 10. Accelerometer scale factor errors

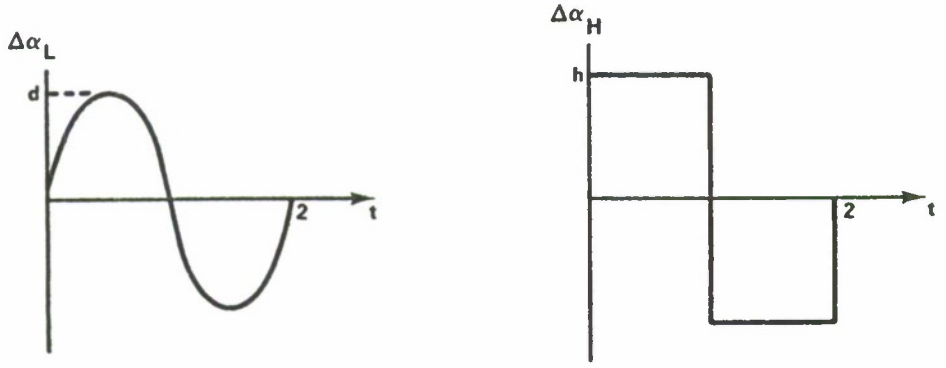

Figure 11. Approximate nonlinearity and hysteresis error curves for a leg mounted accelerometer during kip-up

$$\Delta SF = 0.0204 \text{ volts/rad/sec}^2 \times 1.0^\circ F \times 0.024 \text{ percent}/^\circ F$$

$$\Delta SF = 2.44 \times 10^{-5} \text{ volts/rad/sec}^2$$

which is small compared to the dynamic resolution of the accelerometer.

The hysteresis of the accelerometer encompasses the best fitted straight line scale factor as illustrated in Figure 10 by the dashed curve (cdef). That is, the hysteresis curve produces an envelope about the best fitted straight line scale factor. The hysteresis and resolution value, given in Table I, is less than 0.05 percent of full scale output ($200/\text{rad/sec}^2$). Hence, the value for line segment OC in Figure 10 is:

$$5 \times 10^{-4} \times 2 \times 10^2 \text{ rad/sec}^2 = 0.1 \text{ rad/sec}^2 \quad .$$

Therefore, when the input to the accelerometer, around zero, is increasing or decreasing, the output is in error by 0.1 rad/sec^2 or less. Although the device can detect signals as low as 2×10^{-3} rad/sec^2, the absolute accuracy of the reading is only within 0.1 rad/sec^2. A more graphical illustration of the linearity and hysteresis error effects may be shown by assuming the input acceleration to be a sinusoid. This is an idealization of a leg's angular acceleration during the kip-up. The output voltage error is a sum of the scale factor curve errors or $\Delta e_o = \Delta e_L + \Delta e_H$. A worst case is for the leg's acceleration to be near full scale so that the nonlinearity voltage error is approximately

$$\Delta e_L = d \sin \omega t \quad .$$

The voltage error due to hysteresis is approximately constant for

this input and of the opposite sign of sin ωt. That is,

$$\Delta e_H = -h \text{ sgn } (\sin \omega t)$$

where h = 0.05 percent × SF = 0.1. Now

$$\Delta e_o = \Delta e_L + \Delta e_H = d \sin \omega t - h \text{ sgn } (\sin \omega t)$$

and the acceleration error is approximately

$$\Delta\ddot{\theta} = \Delta e_o/SF = [d \sin \omega t - h \text{ sgn } (\sin \omega t)]/SF \quad .$$

The error in angular rate and angle is obtained by integrating $\Delta\ddot{\theta}$:

$$\Delta\dot{\theta} = (1/SF) \int_o^t [d \sin \omega x - h \text{ sgn } (\sin \omega x)] \, dx$$

$$\Delta\theta = (1/SF) \int_o^t \int_o^t [d \sin \omega x - h \text{ sgn } (\sin \omega x)] dx dt \quad .$$

Because the kip-up motion requires approximately 2 seconds, we take t = 2. Figure 11 shows the shape of the errors over one period, and Figure 12 illustrates the error in the hysteresis after the first integration. Because of the sine nature of Δe_L, it is averaged out over a complete period. Hence, the hysteresis is the most important error source. Figure 13 shows the second integration of the hysteresis acceleration error which grows parabolically with time. Evaluation of the integrals for the rate error and position error due to the hysteresis show that

$$\Delta\dot{\theta}_{H_{max}} = 0.1 \text{ rad/sec} = 5.7 \text{ deg/sec}$$

and

$$\Delta\theta_{H_{t=2}} = 0.1 \text{ rad} = 5.7 \text{ deg} \quad .$$

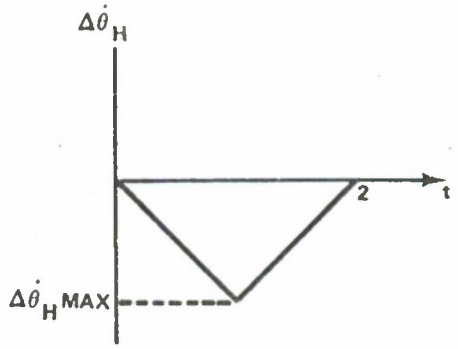

Figure 12. First integration ($\dot{\theta}_H$) hysteresis error

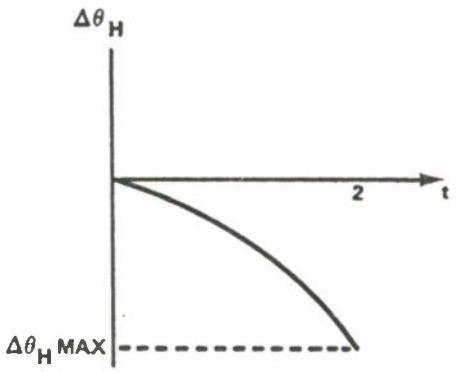

Figure 13. Second integration (θ_H) hysteresis error

The noise value given in Table I is 2.5 mV rms. This noise is assumed white and the integration process will essentially filter out the noise. Thus, the noise will be ignored in the error analysis.

The bias, given in Table I, is generally affected by temperature changes or reflects shifts in the scale factor curve from turn-on to turn-on. However, bias is essentially constant once the accelerometer is in operation and the ambient temperature is relatively constant. The bias value given will produce an offset equivalent to 9.8×10^{-3} rad/sec^2 which is insignificant. Also, this level can be nulled out at the input to the analog computer because of the bias stability. Because it is assumed that the ambient temperature is stable within 1°F during the test period, it may be shown that the bias sensitivity to temperature is insignificant. Repeatibility, i.e., the repeatibility of zero voltage after an acceleration is removed, is given in Table I to be only 0.02 percent of full scale or 0.04 rad/sec^2. Because this error source is bounded by the hysteresis and is much smaller, it is masked by the larger error and is insignificant.

The sensitivity of the accelerometer to linear and off-axis angular accelerations was investigated. Misalignment of the accelerometer will introduce some off-axis angular acceleration and linear accelerations are always present. This error resulting from misalignment is caused by imperfections within the accelerometer and is not related to the resolution problem caused by misalignment. Figure 14 illustrates the simple pendulum and the type of error angles associated with the misalignment. The high bar (POT) and the pendulum arm (OB) establish one plane, then OB and BB' establish a normal plane. It is desirable to align the sensitive axis (AB) of the accelerometer perpendicular to the plane OB-BB' and in the plane POT-OB. However, due to the flexibility of the human limbs and slight initial misalignments, it is virtually impossible to accomplish the ideal alignment. Therefore, error angle ϵ_1 corresponds to misalignment of AB in the plane POT-OB, and error angle ϵ_2 is for misalignment of AB out of the plane POT-OB.

Even if the accelerometer is perfect, these misalignment angles introduce an error in the measured acceleration equivalent to the cosine of the misalignment angle. However the misalignment errors also cause coupling under dynamic conditions by accelerometer imperfections. The angular accelerations induced off-axis are the sines of the angles multiplied by the actual pendulum's angular acceleration, $\ddot{\theta}$. This gives an error in the indicated angular acceleration of $\Delta\ddot{\theta}_{CA} = \ddot{\theta} \sin \epsilon_i$ (3 mV/rad/sec^2)(0.05 rad/sec^2/mV). Since ϵ_i is less than 0.05 rad and the cross axis sensitivity of 3 mV/rad/sec^2 is the maximum, then $\Delta\ddot{\theta}_{CA} < 0.0075\ \ddot{\theta}$. This error is less than 1 percent of the actual acceleration.

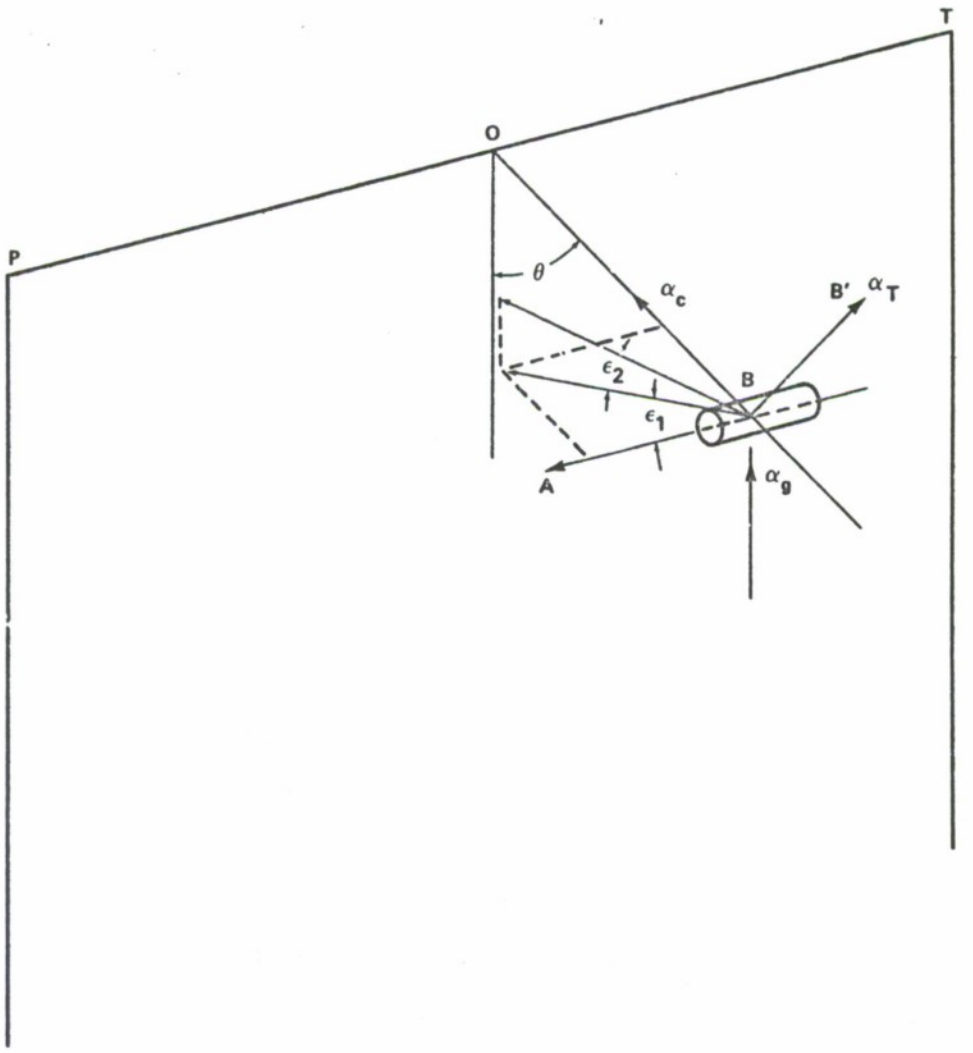

Figure 14. Simple pendulum misalignment angles

The error induced by sensitivity to linear acceleration is

$$\Delta\ddot{\theta}_{LA} = (0.9 \text{ mV/g})(0.05 \text{ rad/sec}^2/\text{mV})a_L$$

where a_L is the linear acceleration of the accelerometer in g's. For a 6-foot kip-up performer, the maximum acceleration is always less than 10 g's at 50 rad/sec^2 and is less than 2 g's for all but 10

percent of the time of motion. Thus,

$$\Delta\ddot{\theta}_{LA}\Big)_{max} < 1.35 \text{ rad/sec}^2$$

for the maximum expected angular acceleration of 150 rad/sec^2 and

$$\Delta\ddot{\theta}_{LA}\Big)_{nan} < 0.09 \text{ rad/sec}^2$$

most of the time of motion. These errors are less than 1 percent of the actual angular acceleration. Hence, if the misalignment can be maintained within ±3 degrees, the measured acceleration should be in error by less than 2 percent of the actual acceleration.

A test plan was devised to evaluate the critical parameters of the accelerometer on an oscillating rate table. After a few test points within each test section, it was evident that the performance of the accelerometer was superior to that of the oscillating rate table. The data collected indicate that the accelerometer is better than the vendor specifications.

EMG and Preamplifiers

EMG and Preamplifier Description

The EMG electrodes originally were part of a system to measure muscle force signals. The EMG electrodes are mounted at strategic points on the muscle group such that a differential force signal can be detected. The electrode element is recessed in a cup-like arrangement such that the cup can be filled with a saline-surgical jelly material to enable a good electrical circuit when brought in contact with the skin. The common element of the differential pair of electrodes is placed at a bony neutral point relative to the two

active elements. The bony point is neutral because of little muscle activity in its area. Due to the very low currents generated in the electrodes, signal detection requires a very high input impedance differential amplifier.

Design Considerations

During preliminary studies, it was assumed that the signal levels from the electrodes would be in the microvolt region. However, this was found to be only partly true. During this preliminary study, the only information available concerning the EMG signal characteristics was that shown in Figures 15, 16, and 17.* These power spectral density curves only present a normalized amplitude and frequency spread. Therefore, it was necessary to develop data that would show how the signal level varied with the duration of time because electrode mounting, variation in signal level from mounting to mounting, and the actual signal bandwidth.

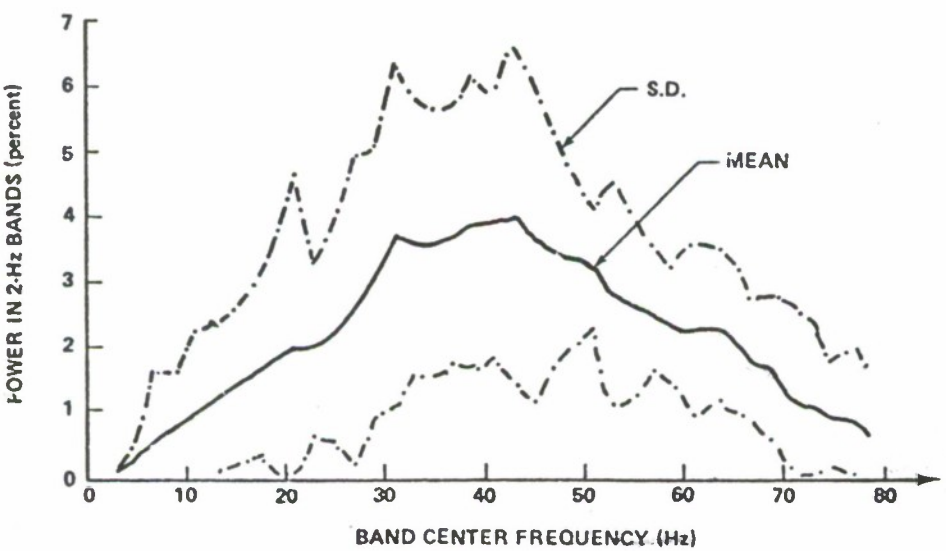

Figure 15. Biceps rested EMG power spectra

*This unpublished work performed by Dr. K. Kilpatrick at the University of Michigan.

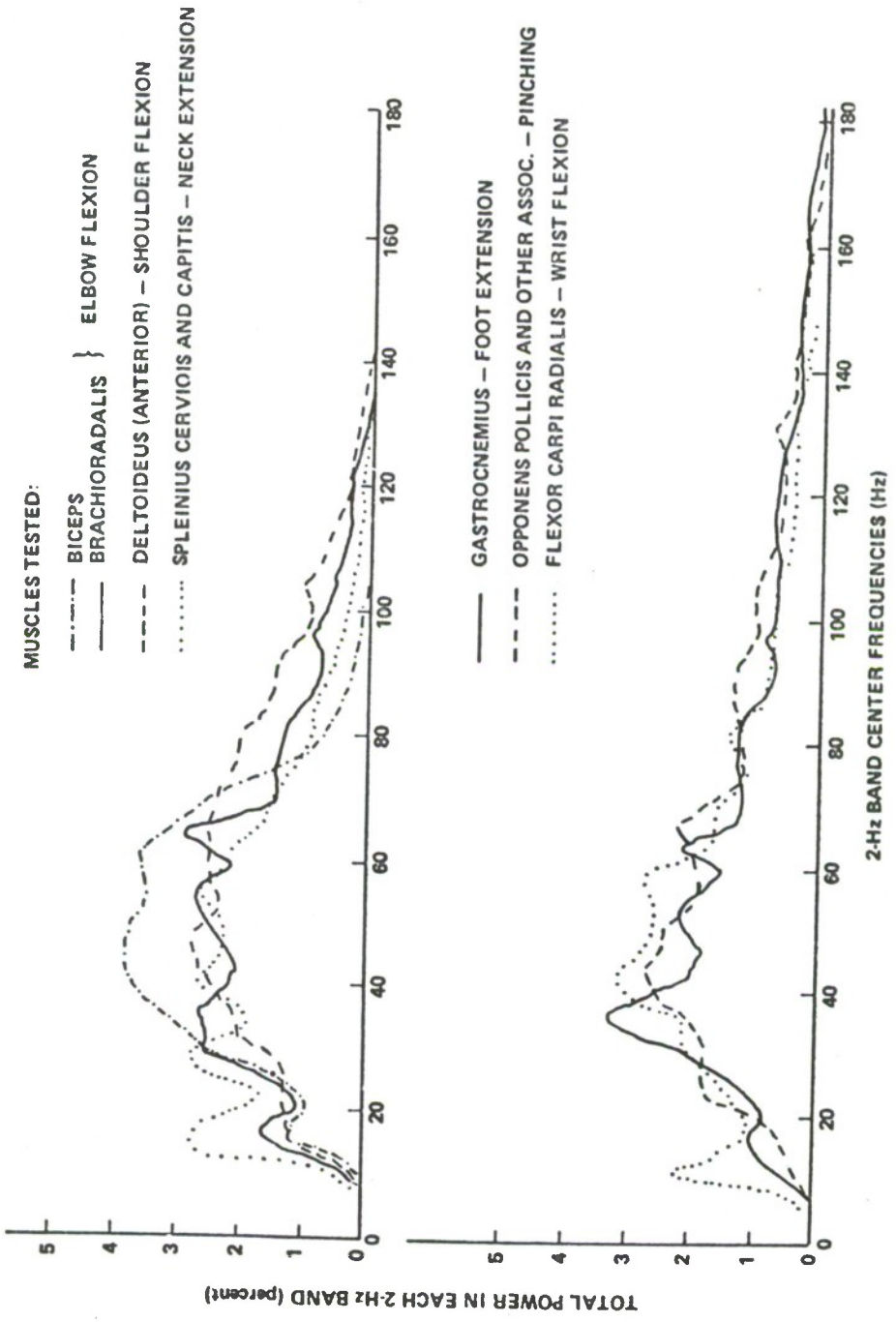

Figure 16. Comparison of different rested muscle EMG spectra

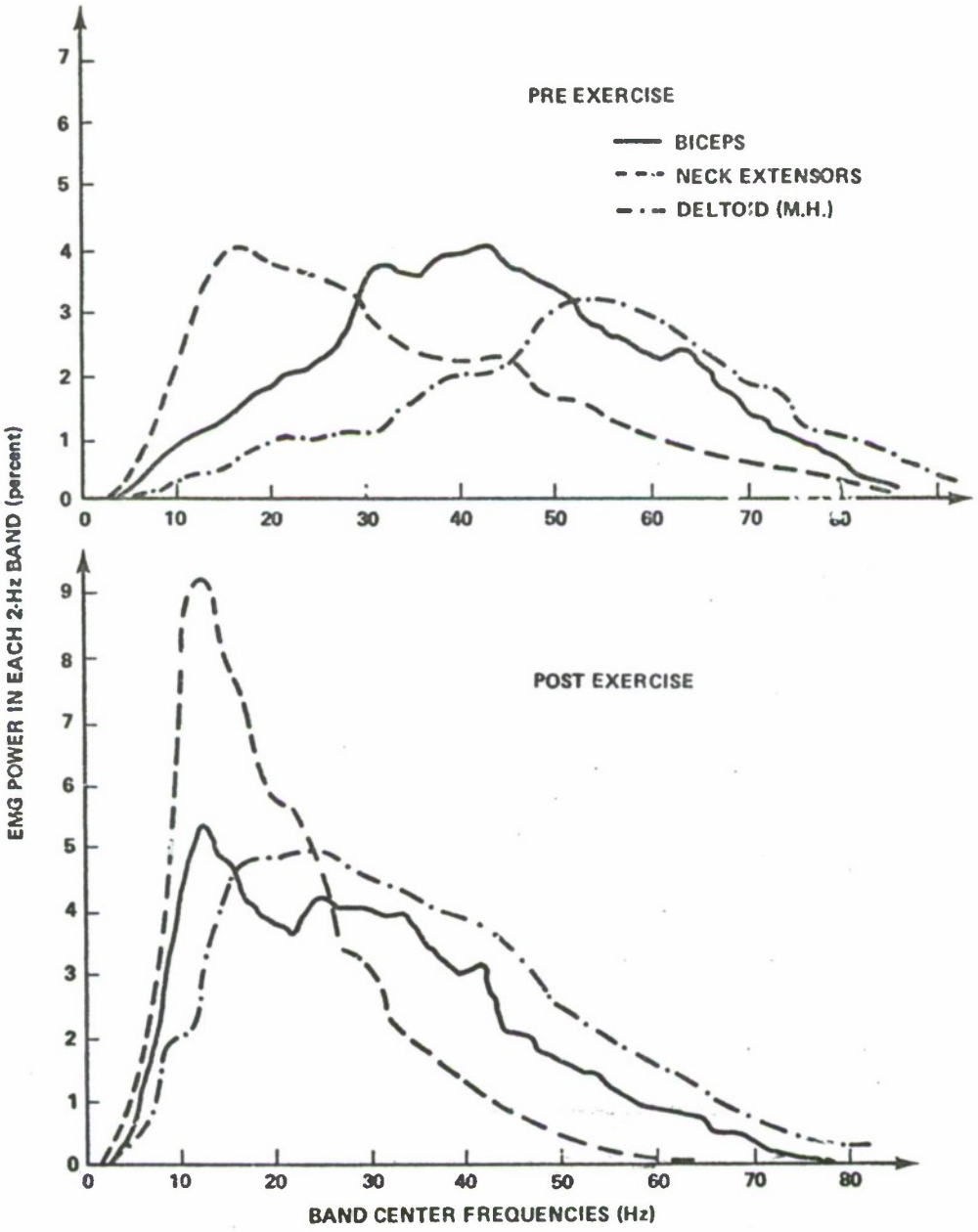

Figure 17. Average spectra before and after fatigue exertions

The composition of the unprocessed signal appeared to be rather random as can be seen in Figure 18.

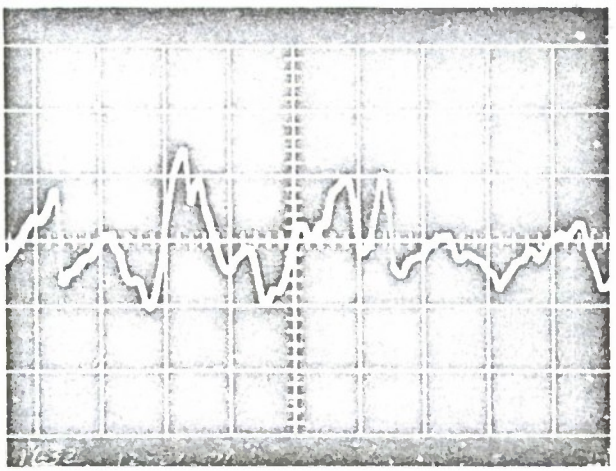

SCALE:
5 volts/cm
10 msec/cm
25 lb LOAD AT
A 30 deg ANGLE

(a)

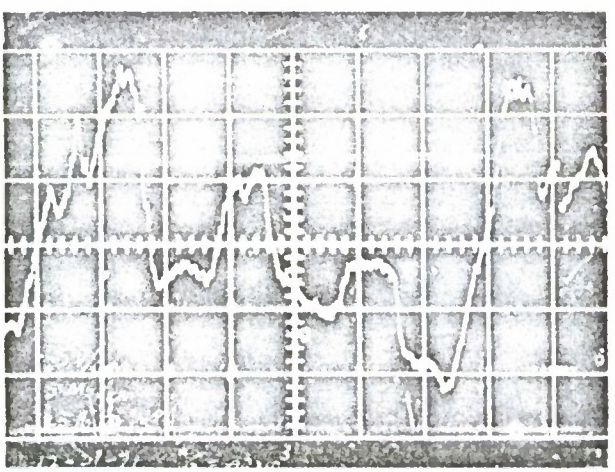

SCALE:
0.5 volts/cm
10 msec/cm
25 lb LOAD AT
A 15 deg ANGLE

(b)

Figure 18. EMG signals with the muscle under load

However, an oscilloscope with a variable pass band differential preamplifier was used to obtain a qualitative figure for the frequency content of the signal (Figure 19). Approximately 90 percent of the signal information is contained in the band of frequencies from 0 to

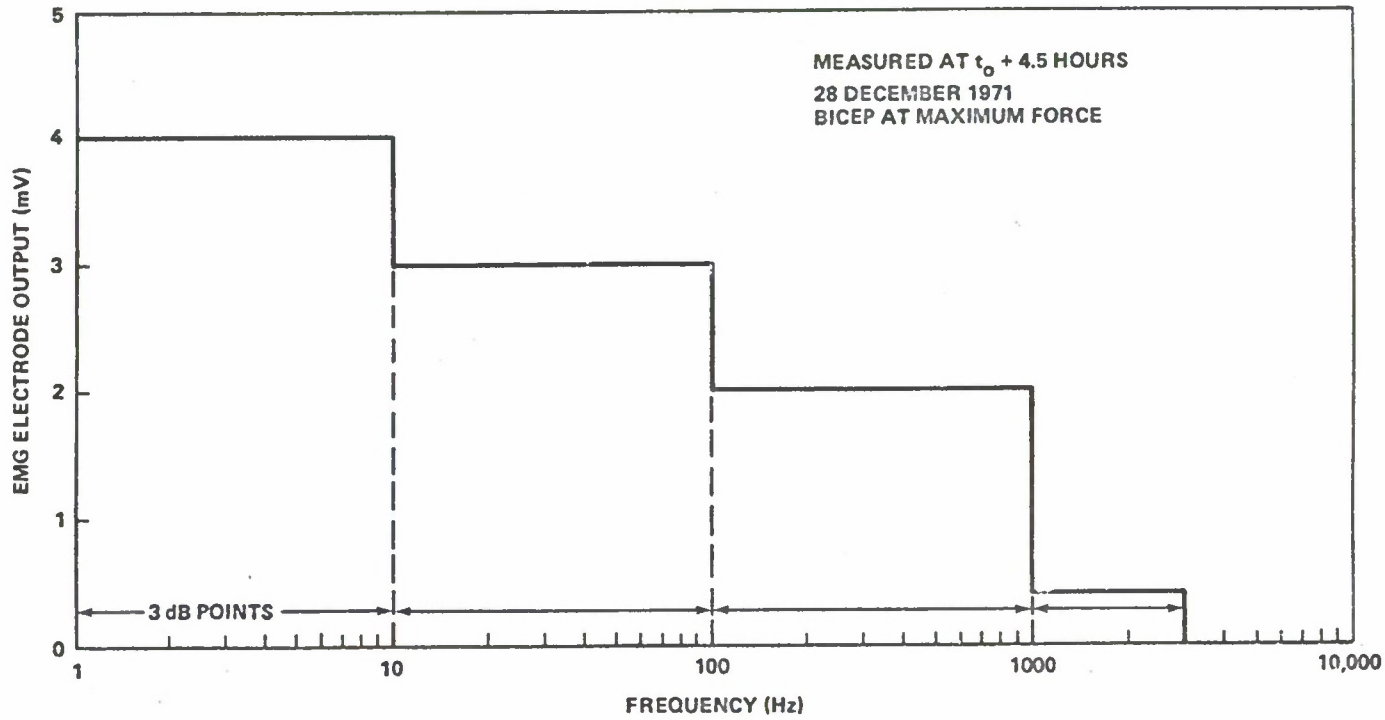

Figure 19. EMG signal output versus frequency measured with a variable bandwidth preamplifier and oscilloscope

1000 Hz. Also, the pass band for the EMG signals will be limited in some cases by the telemetry discriminators' low pass filters. Although the spectral density information indicates that a pass band of 200 Hz would be adequate, it was concluded that an EMG preamplifier pass band of 2000 Hz, which was easily obtainable, would be used.

After establishing a pass band for the EMG electrodes, it was necessary to determine the variation of signal level with time. The electrodes were mounted at time t_o as illustrated in Figures 20 and 21. Also, a preamplifier with a pass band of 2000 Hz and a gain of 1.8×10^4 was used to amplify the EMG signals to a useable level. Figure 22 shows a schematic of this amplifier. At various intervals after the electrodes were mounted, the muscle group was loaded with a 11.3-kg weight (Figure 23) at an angle of approximately 15 degrees. During the interval of the loading, the signal was averaged, in amplitude only, on a storage oscilloscope. This process was repeated for periods up to 12 hours (Figure 20). There is quite a spread in the data points which may be attributed to variations in mounting the electrodes, approximations in the loading angle, and the tone of the muscles being monitored. The variation in mounting emmanated from skin surface condition, the amount of conducting jelly used, and the quality of the contact made when the electrodes were mounted. The skin was dry and clean at the time the electrodes were mounted but other unknown factors could be involved in the mounting process. The amount of jelly used is purely arbitrary. The jelly is squeezed into the electrode cavity such that the cavity will be void free when the electrode is pressed into place against the muscle group. Also, it is desirable to avoid an overflow of the jelly when the electrode is mounted.

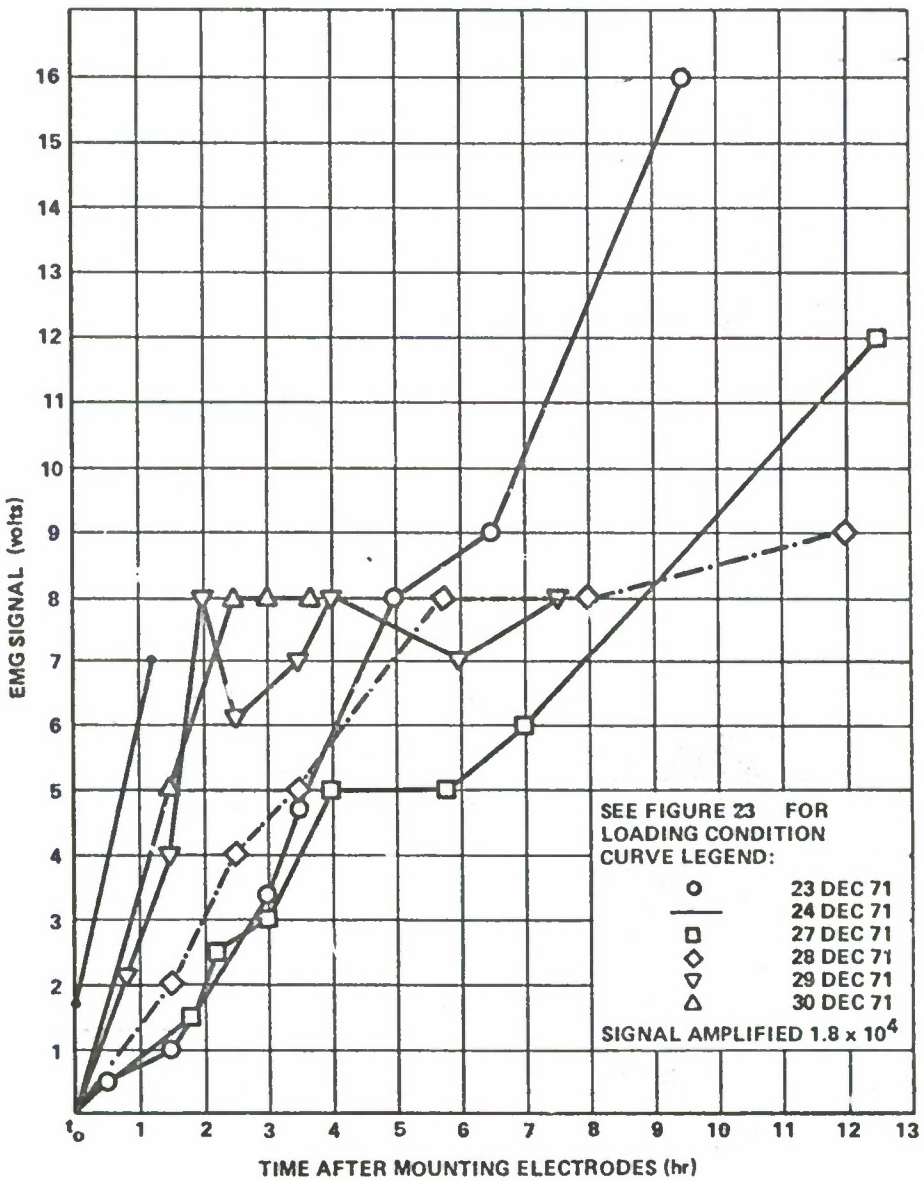

Figure 20. Right arm (bicep) EMG measurement versus time

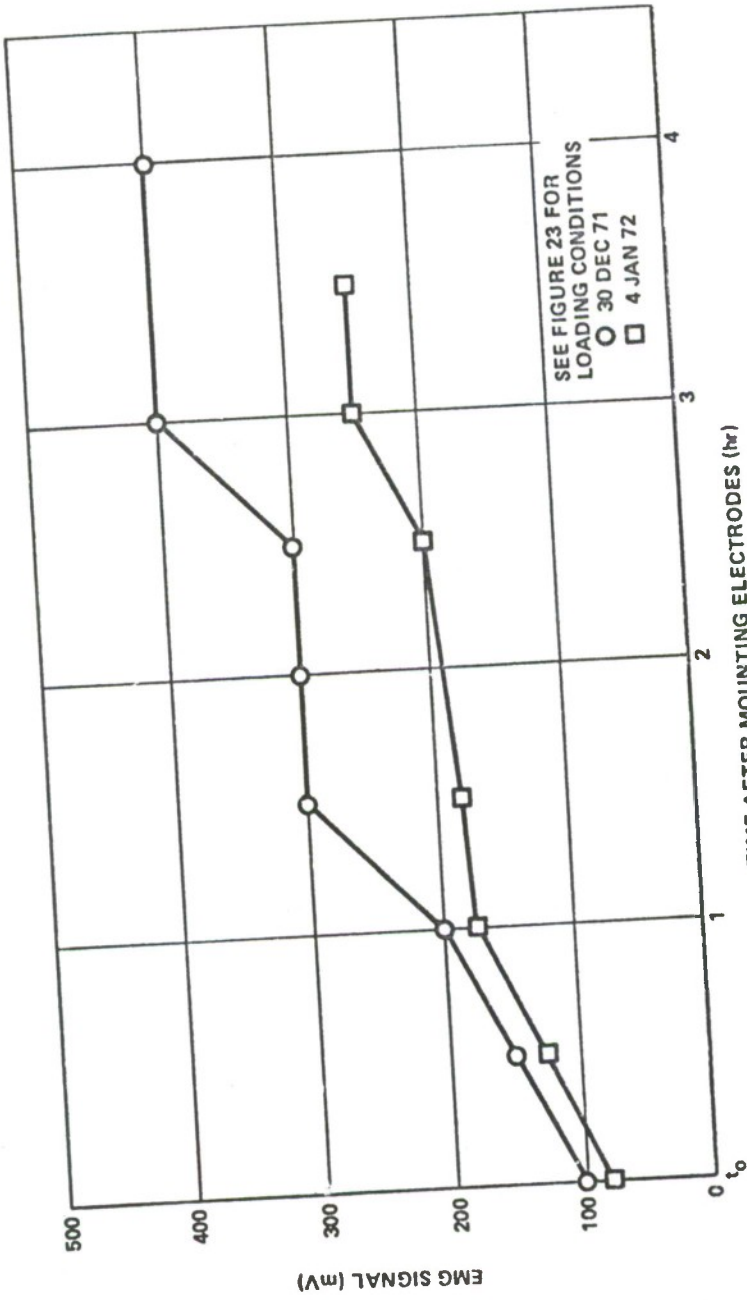

Figure 21. Left arm (bicep) EMG measurement versus time

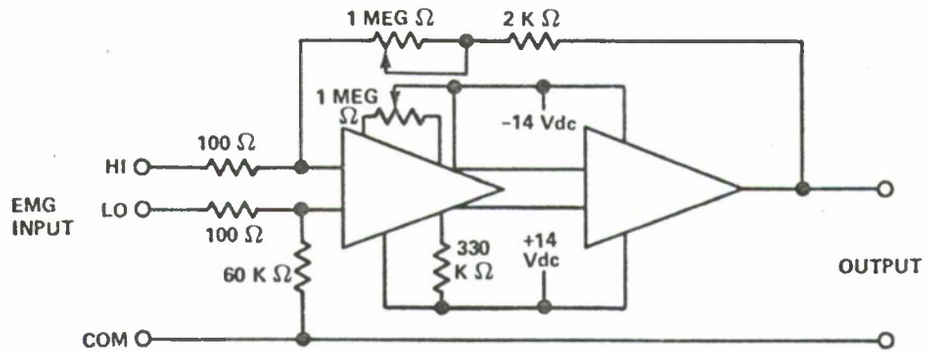

Figure 22. Preamplifier schematic

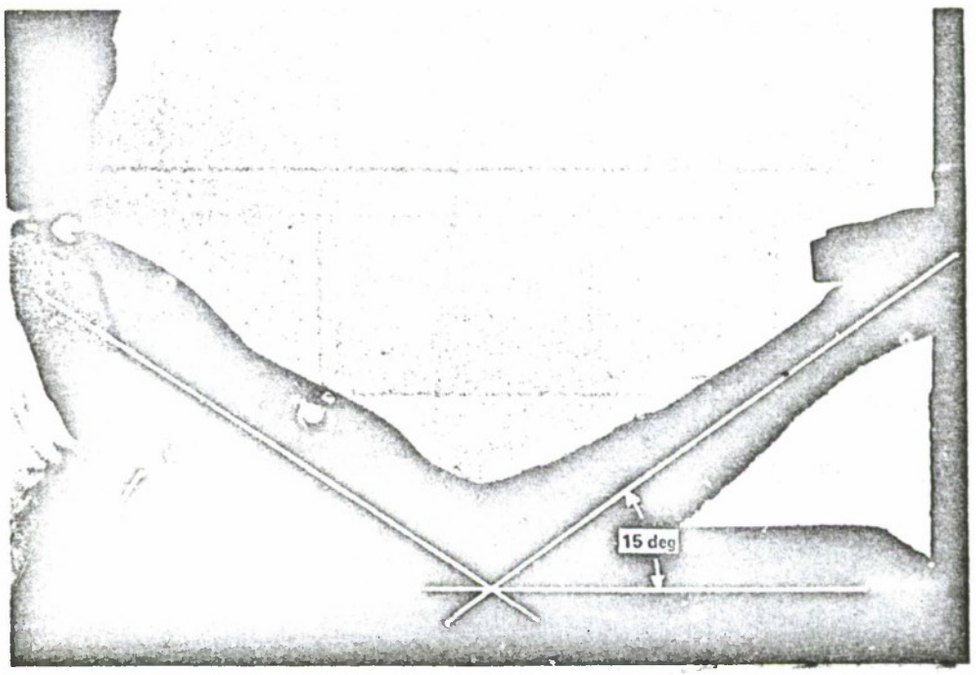

Figure 23. Muscle loading configuration

Once the measurements began, the load angle was an approximation at the best because of the strain on the subject. However, the

distances in Figure 23 were maintained within 3 cm for each measurement. The increase in muscle tone with time produces a marked improvement in the signal level. This may be noted by comparing the improvement in signal level with each new experiment day as shown in Figure 20. Only two sequences of measurements were made with the left arm (Figure 21). It should be noted that the signal amplitude for the left arm was comparable to that of right arm with poorer tone during the first measurements with the right arm. The variation with muscle tone is best reduced by using experienced subjects who have peak muscle tone.

Preamplifier Design

The data collected in this series of tests provided adequate information to design a preamplifier for the EMG electrodes to be used in the instrument system for the body motion measurement study. Also, from these data an error analysis can be performed to establish the accuracy of the muscle signals recorded.

Evaluation of the data collected indicates that the sensors cannot be worn for long periods of time. The curves of Figure 20 indicate that the useful period of a given mounting of the electrodes would be approximately 3 to 5 hours. Also, the EMG signals varied from 27.8 to 80 microvolts over the period. These data were collected from a muscle group having relatively poor tone, therefore, a higher signal level can be expected from a subject with better muscle tone.

Due to the increase in signal level with mounting time of the electrodes and variations in muscle tone from subject to subject, a decision was made to allow calibration of the EMG/preamplifier gain before each test whereby a calibrated, maximum load will be exerted on the muscle group and the preamplifier gain adjusted for a fixed near

maximum level output. The maximum output from the preamplifier is limited by the ±2.5-volt input range of the VCO. Hence, the preamplifier output will be adjusted to ±2.5 volts peak-to-peak for a given maximum load recorded. This maximum load is determined on the force table load cell recording mechanism*. This also will permit correlating signal levels recorded in volts during the kips on the high bar to a specific force level in pounds exerted by the muscle group.

The preamplifier in Figure 22 was designed from the previously mentioned considerations. The gain adjustment permits gains from 20 to 1×10^4 and the bandwidth extends from dc to 2000 Hz. Circuit components, having 5 percent tolerances, enabled a gain stability of better than 0.01 percent. A very high input impedance is realized by virtue of the Field Effect Transistor input circuitry of the Fairchild 727 integrated preamplifier. The Bode' diagram for the preamplifier is presented in Figure 24 and illustrates a performance that is very adequate for its assigned task.

Error Analysis

The EMG error source is confined to signal sensing and the telemetry transmission. The error in sensing will be considered here. Once the EMG preamplifier has been calibrated, the change in signal amplitude with time of the electrode mounting is the primary source of error in measuring the static muscle forces. By referring to Figure 20, it may be noted that curve number 5 has the greatest slope of

$$\frac{\Delta e_o}{\Delta_t} = \frac{4 \times 10^{-4} \text{ volts}}{7.2 \times 10^3 \text{ sec}} = 5.55 \times 10^{-7} \text{ volt/sec}$$

*This force table is described in a thesis by Samras [8].

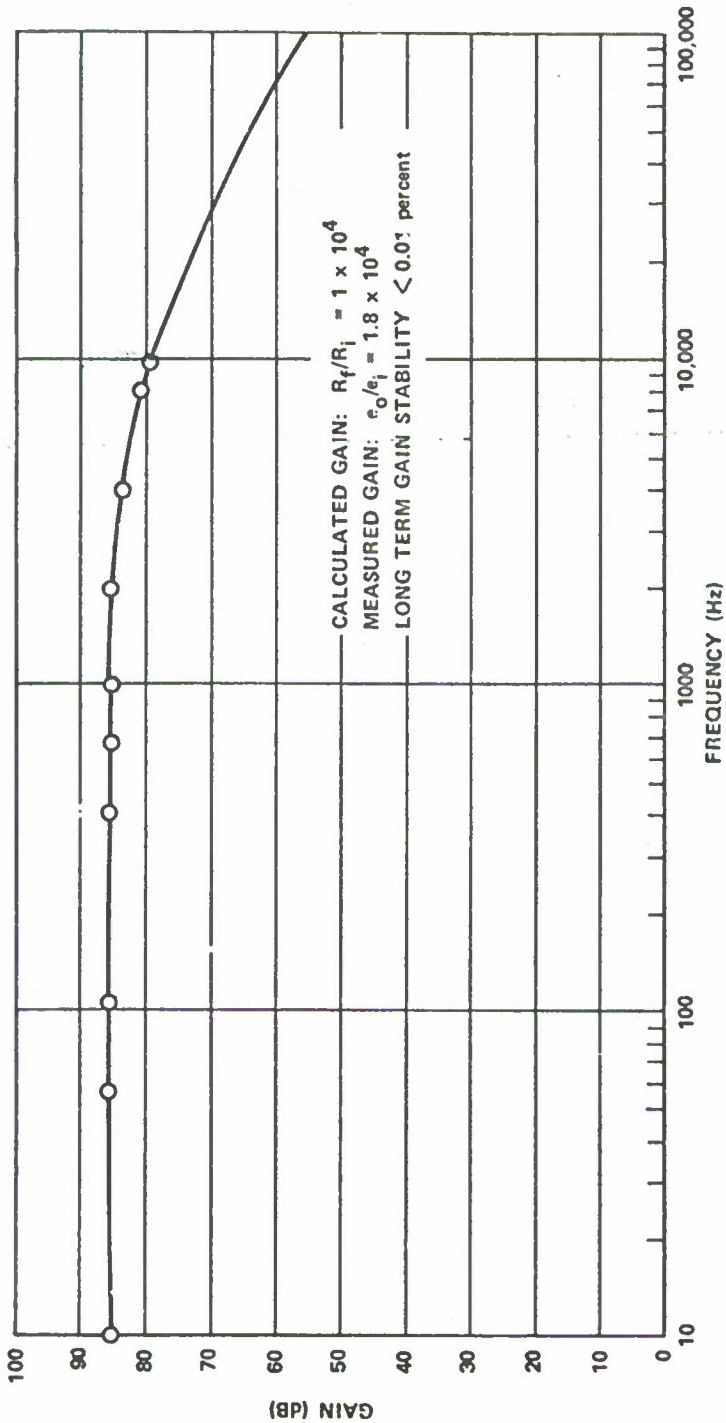

Figure 24. EMG preamplifier Bodé diagram

This error factor will degrade the muscle force data by less than 3.3×10^{-3} percent for a 1-volt signal if the kip on the high bar can be completed within 10 minutes after the calibration on the force table. Since the rate of change for the EMG signal is relatively linear over a nominal 3-hour period, a correction factor can be employed to reduce the error associated with the EMG measurements if needed. However, it is clear that this should not be required.

Telemetry System

Telemetry Error Analysis

The telemetry system used in this experiment is a proportional bandwidth, subcarrier frequency modulated type of mechanization. The amplitude of the modulating signal determines the percentage modulation of the transmitter which should be approximately 60 percent or less.

Mobile Component Description

The telemetry system is comprised of standard IRIG elements. Channels 10 through 21 were selected for the 12 channels employed in this system primarily because of the pass band characteristics of these channels. In conjunction with the channels selected, a P-band solid state transmitter that radiates at 231.9 MHz was available for use in the instrument package. The signal converters are VCO, Conic Corporation, model CSO-220-1. The VCOs have an input range of ±2.5 volts that is converted to an output frequency proportional to the input voltage.

Channel 10, the lower pass band channel, has a center frequency of 5.4 kHz that varies ±40.5 Hz and has a pass band of 80 Hz while channel 21 has a center frequency of 165 kHz that varies ±1235 Hz and has a pass band of 2470 Hz. Each VCO has an adjustment to permit

trimming the voltage sensitivity, the center frequency, and the output amplitude. The outputs of the VCO's are manifold into a mixer amplifier, Conic model CMA400A. In the mixer amplifier, all 12-VCO signals are mixed into a composite signal which modulates the P-band transmitter.

The transmitter, Conic model CTM-402, operates at 231.9 MHz with a 28-Vdc power input. The output is approximately 200 mW. The transmitter uses a quarter wave stub antenna that is approximately 31.5 cm long. The antennea is mounted on a stand-off insulator such that the shielding of the telemetry package will act as a ground plane (Figure 25).

Power for the instrument package will be supplied by four 500-mA/hr Ni-Cad batteries. The EMG preamplifiers require approximately 20 mA per preamplifier and the six accelerometers require 20 mA per accelerometer from the ±14-Vdc supply while the transmitter and VCO's load the 28-Vdc supply at 350 mA. This requires a total power of 1.2 watts. Currently, the supply batteries can provide 14 watts for 1 hour without significant loss in voltage.

Receiver Section Description

The receiving section of the telemetry system employs a Defense Electronics model GPR-20 receiver that has a bandwidth of 1 MHz and a video output of 5 mV/kHz. The video signal output in turn is routed into a bank of 12 Defense Electronics, model SCD 11, discriminators.

The discriminator selects a unique subcarrier signal from the composite video signal, demodulates, and filters the signal into its original state. The low pass filter assures that the carrier components are absent from the analog signal output. The

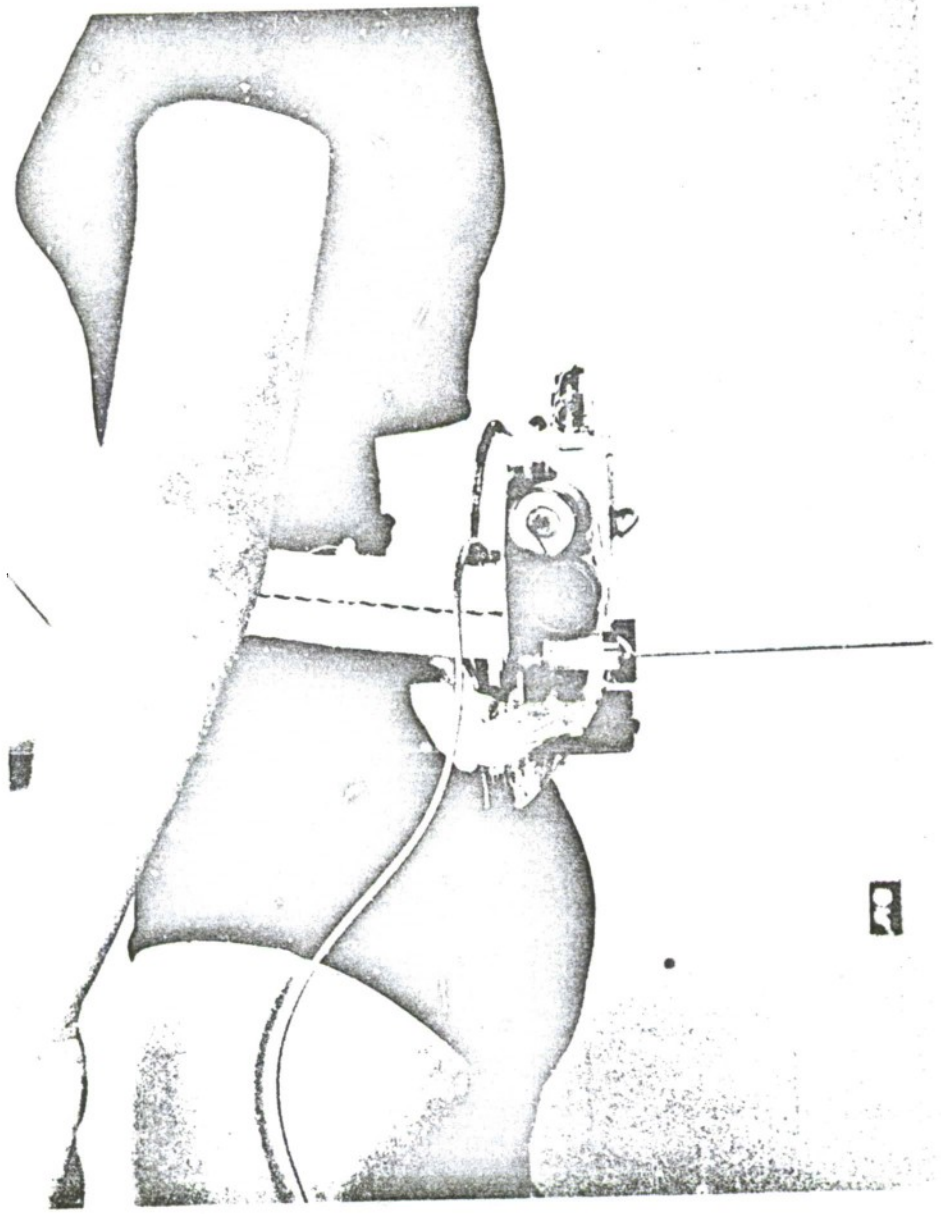

Figure 25. Telemetry package

discriminator has a 60-dB noise rejection and a bandwidth linearity of 0.05 percent. The center frequency is stable to within 0.05 percent

after a 15-minute warm-up. The analog signal output is adjustable from 0 to ±10 volts for full bandwidth deviation.

The error parameters for the VCO's and the mixer, determined experimentally, show that the linearity is better than 0.08 percent and the center frequency stability (Δf_c) is better than 0.037 percent (Figure 26). The error parameters for the receiver and discriminators were extracted from the vendors specification sheets.

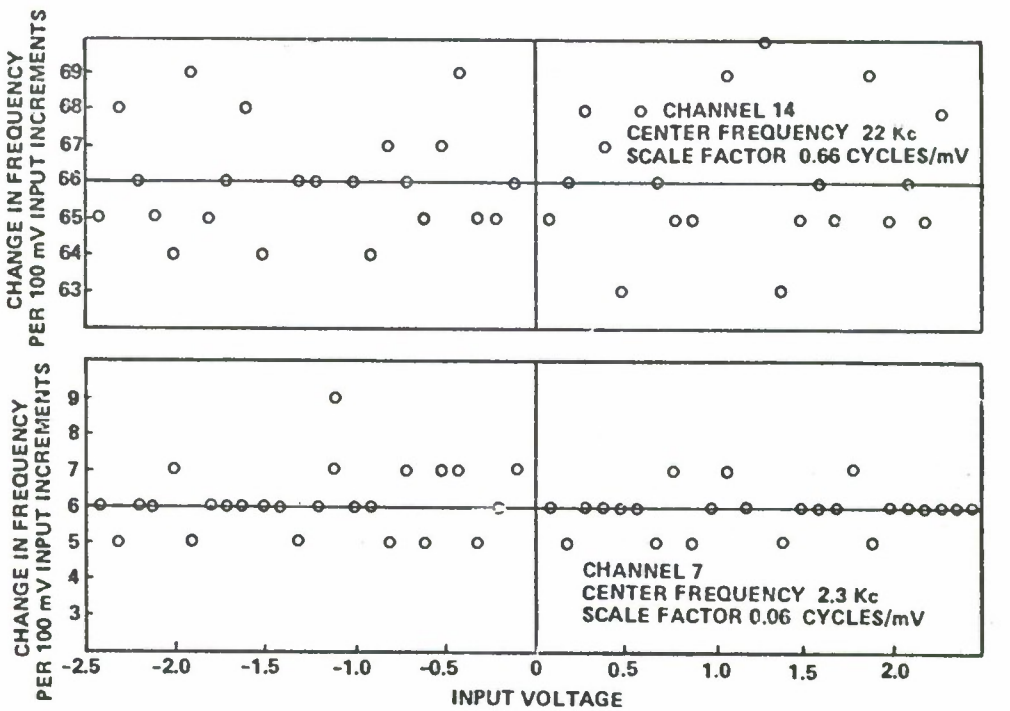

Figure 26. Variable frequency oscillator nonlinearity

The errors for the telemetry system will be assimilated, in a somewhat standard and accepted way, by a root sum square to reflect a composite error figure. The error components to be considered are: center frequency stability (Δf_c), VCO nonlinearity (Δnl), discriminator

linearity (Δdnl), and the discriminator frequency stability (Δf_d). The center frequency variations act like a bias which may vary the position of the input/output curve for the telemetry system. The linearity is a relatively constant value for a given component; however, it may vary with temperature. The root sum square of these errors is

$$e_{tm} = \sqrt{(\Delta f_c)^2 + (\Delta nl)^2 + (\Delta dnl)^2 + (\Delta f_d)^2}$$

$$= \sqrt{(3.7 \times 10^{-4})^2 + (8.7 \times 10^{-4})^2 + (5 \times 10^{-4})^2 + (5 \times 10^{-4})^2}$$

$$= 11.8 \times 10^{-4} \times 100 = 0.118 \text{ percent}$$

Thus the total error contributed by the telemetry system is 0.118 percent.

System Errors

The errors of the various subsystems associated with the body motion instrument system have been investigated but now a figure of merit for the entire system must be derived. Again, the root sum square will be used to arrive at a system error figure.

Since the magnetic tape recorder will be used for data storage, an error value for the tape system is included and is denoted by e_{ta}. Then the composite accelerometer loop error is the hysteresis error e_H, the telemetry error e_{tm}, and the recorder error e_{ta}.

The record amplifier has a temperature stability of 0.4 percent and and a frequency stability of 0.2 percent while the reproduce amplifier has a nonlinearity of 0.25 percent peak-to-peak of the best fitted

straight line through zero and a temperature sensitivity of 0.3 percent. The root sum square value of the errors for the tape recorder is

$$e_{ta} = \sqrt{\left(3 \times 10^{-3}\right)^2 + \left(2.5 \times 10^{-3}\right)^2 + \left(2 \times 10^{-3}\right)^2 + \left(4 \times 10^{-3}\right)^2}$$

$$= 0.6 \text{ percent} \quad .$$

The system error for these subsystem errors is then

$$e_s = \sqrt{e_{ta}^2 + e_{tm}^2 + e_H^2} = \sqrt{(0.6)^2 + (0.118)^2 + (0.125)^2}$$

$e_s = 0.625$ percent the total system error

CHAPTER III. SYSTEM EVALUATION

Introduction

A theoretical evaluation of the system and its constituent parts has been completed from data having various origins. Now the subsystems are integrated into the total system and evaluated as a system.

Initially the system was measured for linearity and frequency response without the sensors. This phase of the evaluation substantiated the theoretical development for the telemetry and the data storage equipment.

Next the dynamic measurements were made with the instrumented subject swinging on the high bar. This phase was partitioned into two sets of measurements because of the limited supply of accelerometers and active telemetry channels.

System Linearity and Frequency Response

System Linearity Test Description

The overall system accuracy without the sensors was evaluated for linearity and hysteresis. The test was performed with the system configured as shown in Figure 27. The signal source was varied in 500-mV steps between ±2.5 volts and monitored on a digital voltmeter. Tables II and III contain the data obtained from this test with and

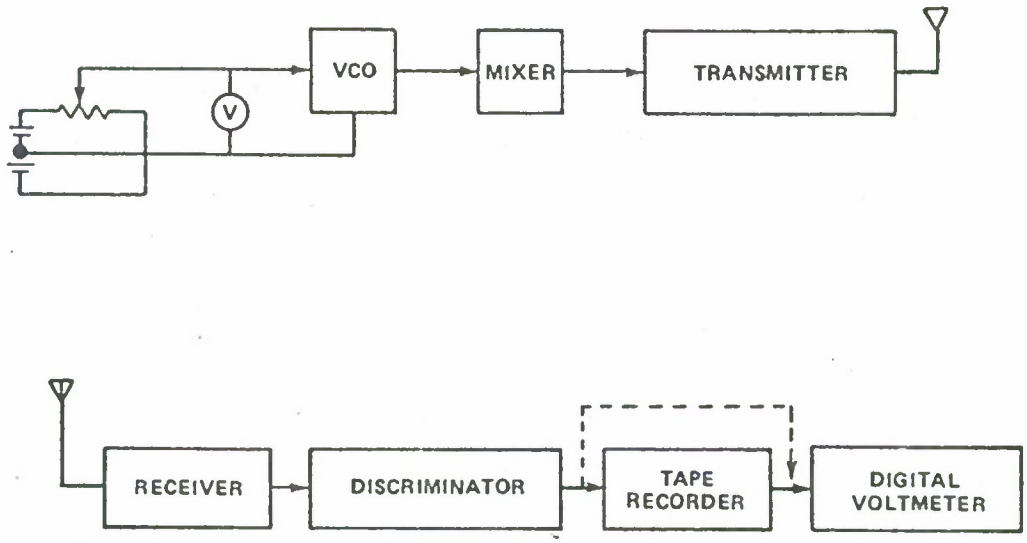

Figure 27. Block diagram for system linearity test

Table II. System linearity without the tape recorder

Input Voltage (volts)	Output Voltage (volts)
- 2.500	- 2.509
- 2.000	- 2.011
- 1.500	- 1.499
- 1.000	- 1.007
- 0.500	- 0.495
0.000	- 0.008
0.500	0.505
1.000	1.000
1.500	1.506
2.000	2.005
2.500	2.506

Table III. System linearity

Input Voltage (volts)	Output Voltage (volts)
- 2.500	- 2.513
- 2.000	- 1.994
- 1.500	- 1.489
- 1.000	- 1.009
- 0.500	- 0.500
0.000	0.000
0.500	0.500
1.000	1.000
1.500	1.500
2.000	2.000
2.500	2.513

without the tape recorder in the system. Some instability was encountered due to RF coupling into the modulation circuitry. However, this was overcome by shielding.

System Frequency Response Test Description

In conjunction with the system evaluation, a frequency response was obtained for channels 10 and 14 which were the lowest frequency and highest frequency channels presently available. Figure 28 illustrates the configuration employed for the frequency response analysis. The oscillator output was maintained at 1 volt peak-to-peak while varying the frequency over the spectrum of interest. The frequency response was measured for channels 10 and 14. Figures 29 and 30 illustrate the pass band for channels 10 and 14, respectively.

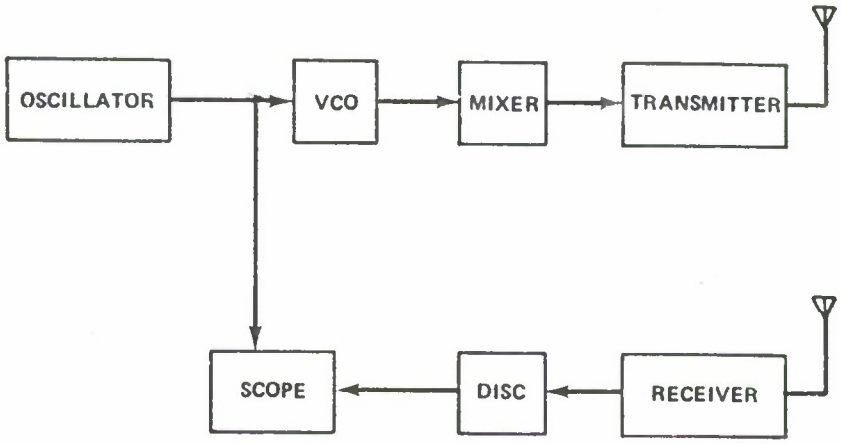

Figure 28. Block diagram for system frequency response

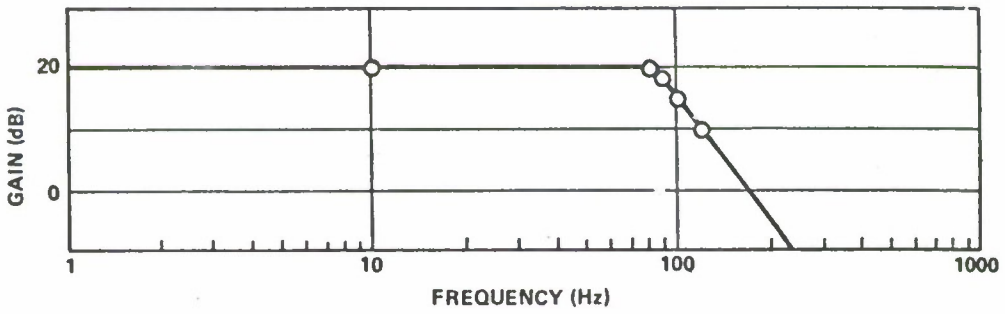

Figure 29. Channel 10 frequency response

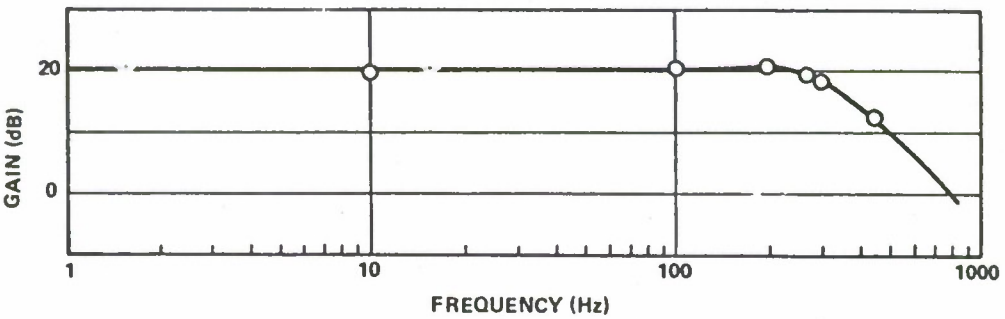

Figure 30. Channel 14 frequency response

In reference to the pass band specified for the discriminators, it is significant to note that the Bode' diagrams for the two channels reflect the discriminator filters exactly.

Static Linearity Analysis

The telemetry system was connected as shown in Figure 27 without the tape recorder box. Linearity of the system was measured by varying the input signal between -2.5 and +2.5 Vdc while recording the output of the system on a digital voltmeter. Table II presents the data recorded from channel 10. It was assumed that the higher numbered channels would be at least as good as channel 10; therefore, channel 10 was considered representative for the system.

At -2.000-volts input the greatest departure from a straight line is 11 mV. Hence, the measured error e_{tm} is

$$e_{tm} = \frac{\Delta e_o \text{ max}}{e_i} = \frac{11 \times 10^{-3} \times 10^2}{2} = 0.5 \text{ percent} .$$

This actual measured error is approximately four times greater than the calculated error of Chapter II. Subsequently, the system of Figure 27 was employed with the tape recorder to measure the linearity for the entire system. The technique was the same as that without the tape recorder. Table III presents data measured from channel 10. The maximum departure from a straight line was 13 mV for the system. However, the greatest error appears at the maximum input point which should be greater than the maximum signal encountered during an actual test. The system error calculated from these data is

$$e_{sys} = \frac{e_o \text{ max}}{e_i} = \frac{13 \times 10^{-3} \times 10^2}{2.5} = 0.52 \text{ percent} .$$

This is less than the value of overall system error previously calculated.

Dynamic Evaluation

Arm Link Test Description

Measurement of the arm link accelerations and muscle forces was conducted as illustrated in Figure 31. The accelerometer was mounted in the bracket shown at A and the EMG electrodes were mounted on the bicep muscle group as indicated at point B. The system integration for the dynamic phase of the evaluation is shown in Figure 27 with the signal source replaced by the accelerometer and the EMG electrodes.

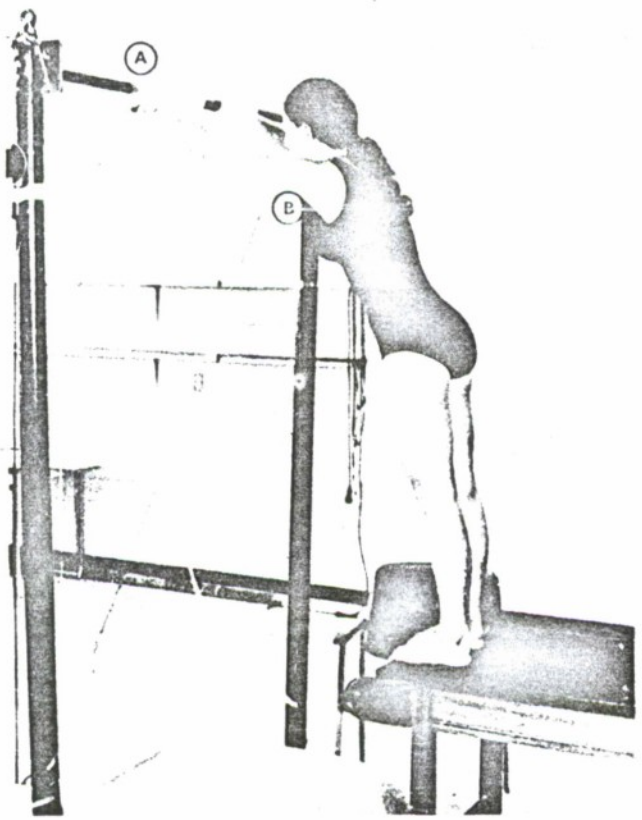

Figure 31. Accelerometer scale factor errors

In preparation for the test, the EMG electrodes were mounted on the subject approximately 30 minutes before mounting the high bar. Along with the electronic mechanization, a movie camera (16 mm) was positioned such that all planar motion of the subject on the high bar was recorded on film during the swinging motion. This photographic record was synchronized with the recorded electronic data. The synchronization was accomplished by pulsing a strobe light with an 18-msec pulse every 170 msec. This pulse width insured that the shutter would be open during at least part of the pulse. The 170-msec period corresponded to a flash about every 10 frames. The same pulse that energizes the strobe light was recorded on one channel of the tape recorder. The ability to correlate the photographic record with the electronic data recorded permits an accuracy time correlation of the two data sources.

After the equipment setup was complete and the EMG mounting was aged, the subject loaded the bicep muscle group to a maximum. While the muscle group was under a known load, the gain of the EMG preamplifier was adjusted for a ±2.5-volt peak-to-peak reading on an oscilloscope.

Upon completing the EMG calibration, the subject moved immediately to the high bar where the accelerometer was connected into the instrument package. Before the first movement, the recording equipment was started and at first movement, the timing signals were initiated. At least four cycles of data were recorded for each test.

Leg Link Test Description

The leg link measurements employed only the accelerometer because of the alignment procedure associated with the accelerometer. The leg

measurements were the same as for the arm except the EMG portion is excluded and the alignment procedure is added.

The alignment of the accelerometer required orienting the sensitive axis of the accelerometer, mounted in the gimbaled bracket on the leg, parallel to the high bar. The alignment was accomplished with a laser having its beam accurately aligned parallel to the high bar by essentially translating the laser axis parallel to the bar's axis. The laser beam was oriented such that the beam impinged on a mirror mounted on the end of the accelerometer. The surface of the mirror was perpendicular to the sensitive axis of the accelerometer. Figure 32 illustrates the configuration that was employed and graphically shows the accuracy realized in the technique.

The laser was located approximately 20 meters from the mirror and had a screen located immediately in front to act as a target board for the reflected laser beam. The screen had a small hole to allow passage of the laser beam to the mirror. The two misalignment angles were calculated by this technique and the gimbal mounting bracket rotated to minimize the misalignment. Figure 33 shows the angles for the equations to calculate the angles.

Once the alignment of the accelerometer was established, the measurement procedure was similar to that of the arm. Upon completion of the dynamic measurements, the data, stored on magnetic tape, were processed in an analog computer to obtain the angular rate and displacement of the given body links measured. Figure 34 shows the computer configuration used to process the data and the strip chart recorder used for storing the processed data.

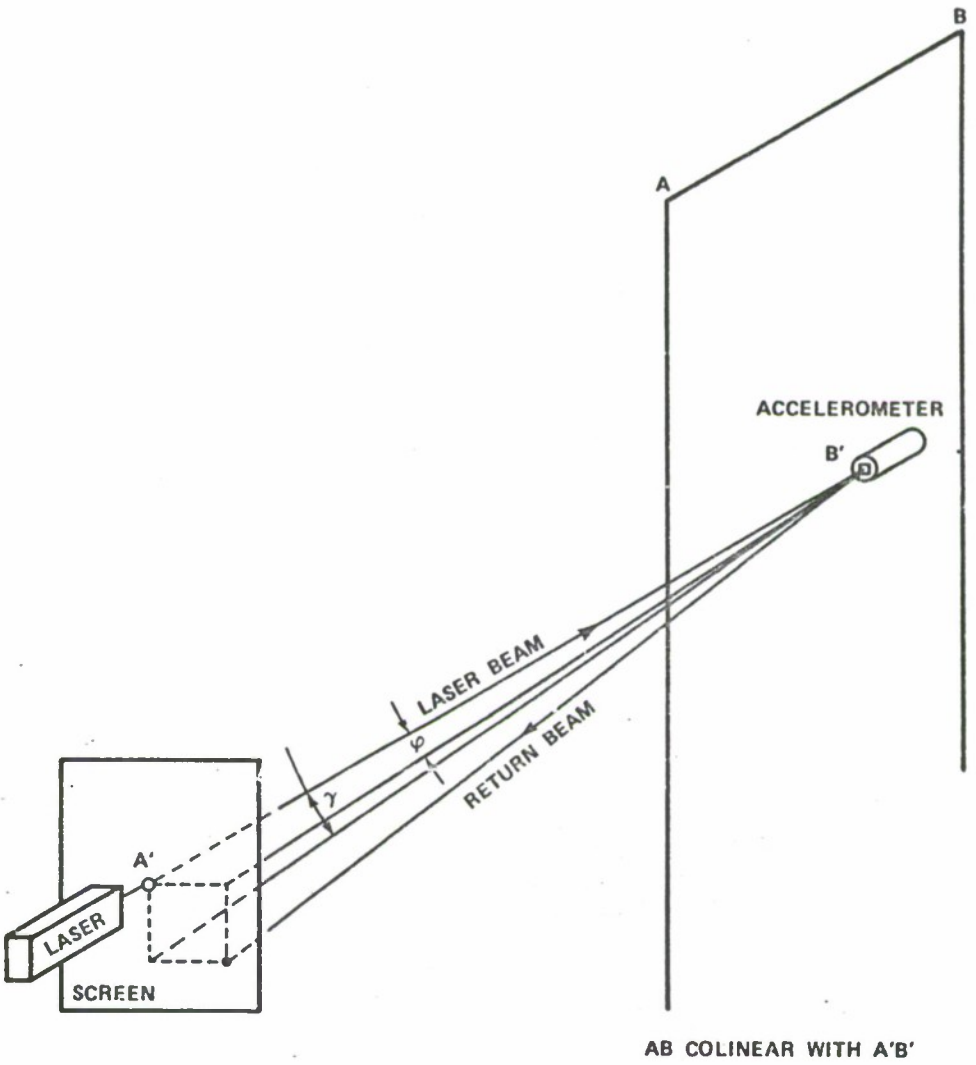

Figure 32. Laser alignment scheme and error angles

The proof of the analysis is in the comparison of the displacement data from the accelerometer and the subsequent integrations and the displacement data from the photographic source. The displacement data obtained from filming are considered to be quite accurate if sufficient care is taken in taking the data from the film.

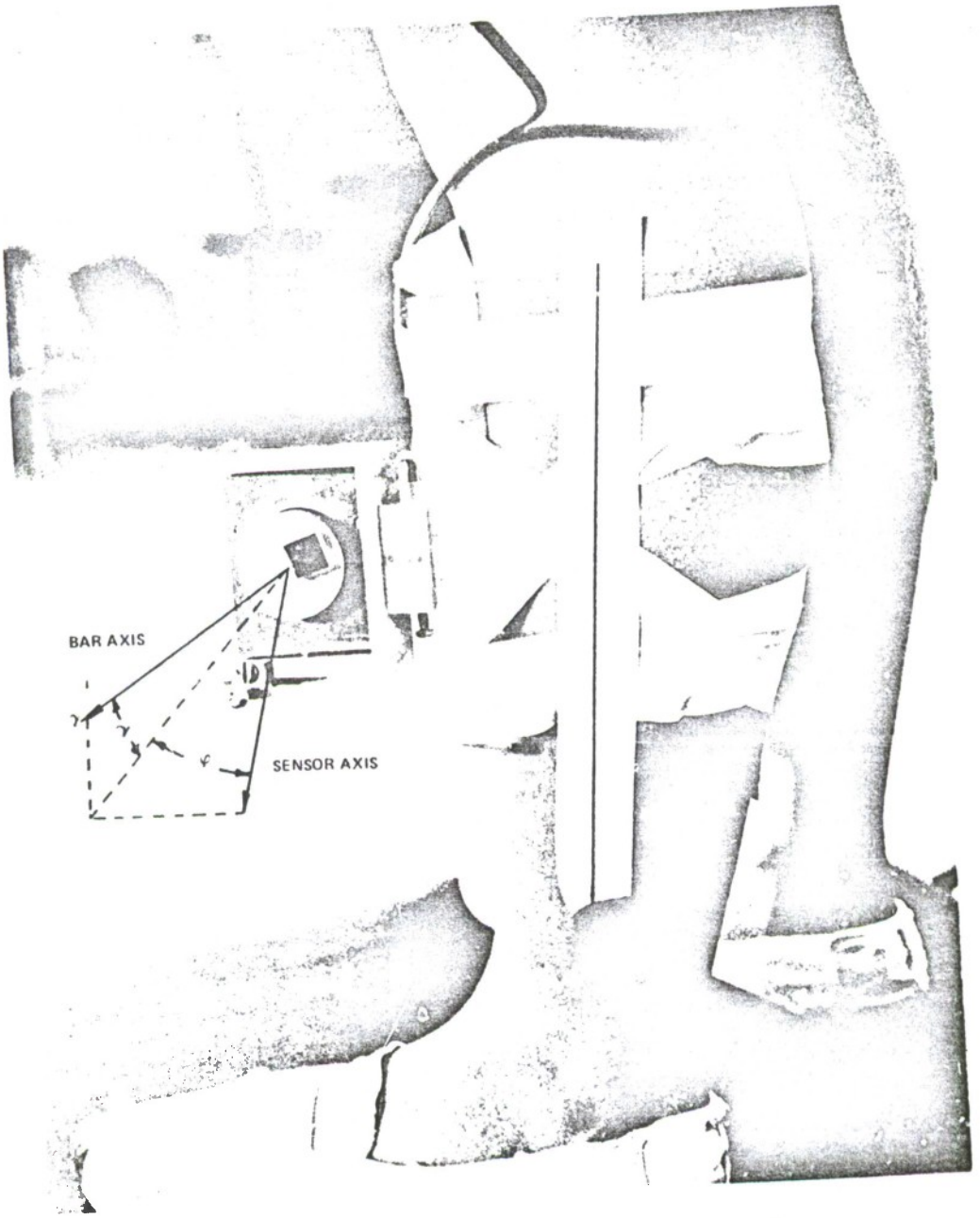

Figure 33. Leg mounting misalignment angles

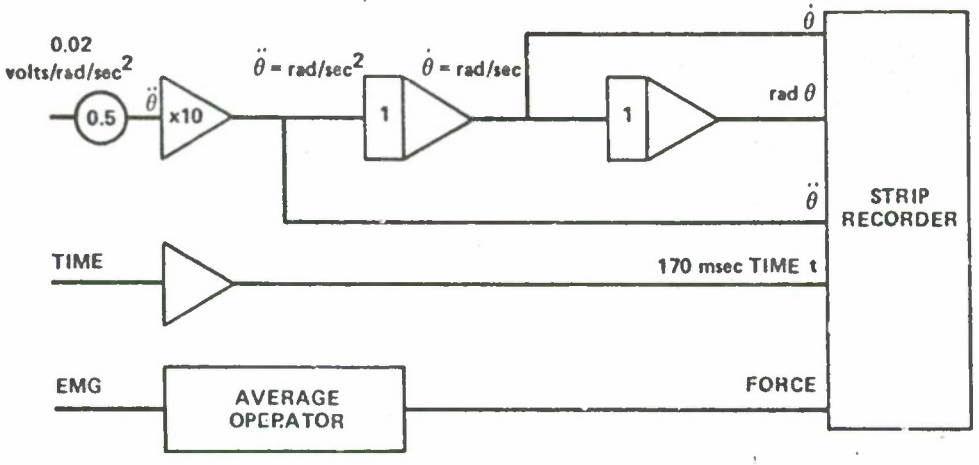

Figure 34. Analog computer program for data reduction

Measurement Evaluation

The dynamic phase of the first experiment was completed with Murphy's law prevailing. The EMG electrodes were swamped with RF energy which yielded this portion of the data useless. Also, after looking at the data stored on the magnetic tape, it was found that the 28-Vdc supply failed to maintain an adequate voltage level for the duration of the test.

In contrast to the problems encountered, the procedure for conducting the experiment was satisfactory. The arm acceleration measurement was inherently void of alignment problems and the implementation of this phase of the experiment offered no special attention. The mounting and alignment of the accelerometer on the leg proved to be better than expected. Translation of the longitudinal axis of the high bar with the laser was accomplished within 2 minutes of arc. This established a reference axis with which the accelerometer could be aligned without significant errors. Also, the subsequent alignment of the accelerometer to this reference axis is shown in Figure 35.

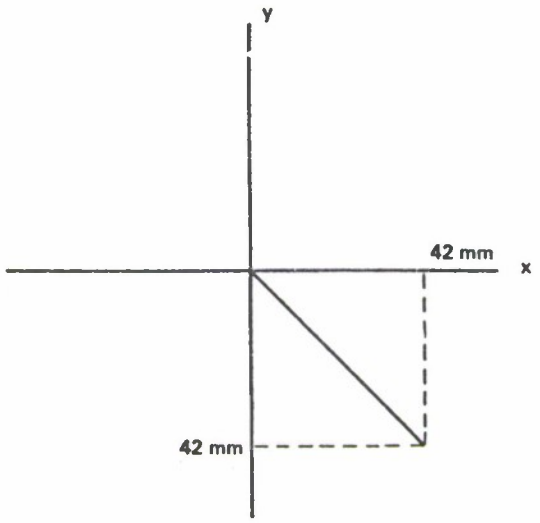

Figure 35. Misalignment errors in the accelerometer leg mounting

The displacement values given in Figure 35 and a laser baseline of 15 meters produce errors 1 degrec, 37 minutes for angles γ and φ. In observing the subject's motion on the bar in the motion picture film, it appeared that the alignment angles would be maintained within 4 degrees through the motion.

A bench power supply was used to replace the faulty 28-Vdc Ni-Cad battery supply. Although the telemetry package was not completely isolated in its environment, the principle was proven. Thus by replacing thc 28-Vdc supply with new batteries, completc isolation was achieved.

This attempt proved to be fruitful. The leg mounting experiment was evaluated first because the maximum acceleration would be encountered at the leg and thc accelerometer's maximum range would be verified. Figure 36 presents thc data for the leg measurement including the accelerometer's raw data and that processed with the

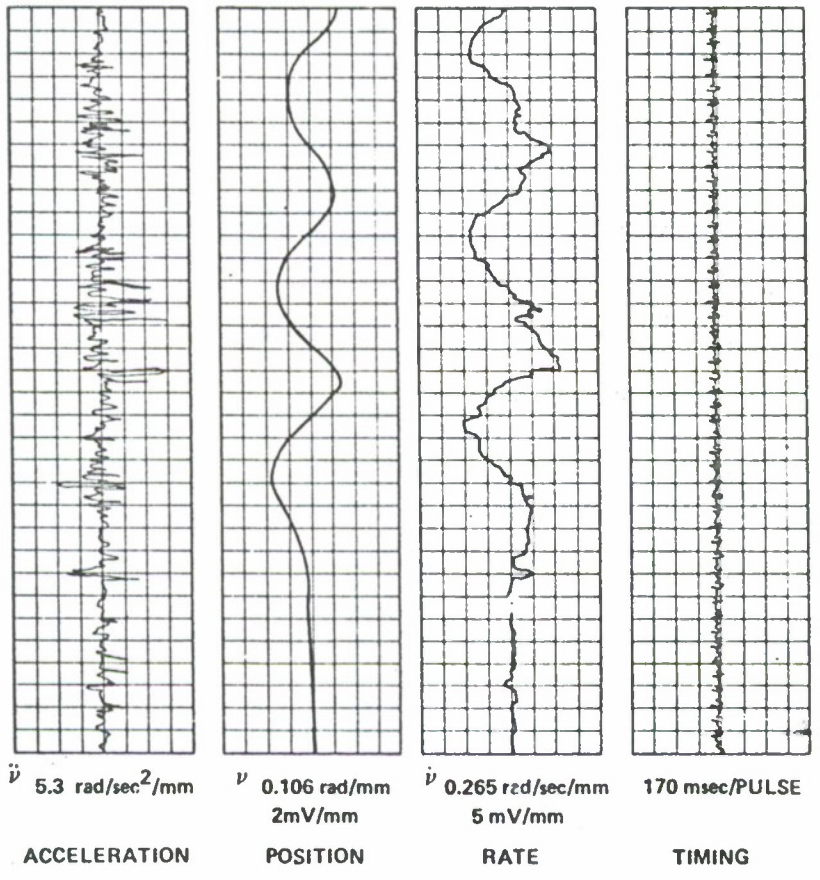

Figure 36. Leg link accelerometer data

analog computer (Figure 37). There are irregularities in the acceleration data ($\ddot{\theta}$); however, their occurrence can be verified in Figures 8 and 38. These irregularities are smoothed extensively after the second integration when the position angle is obtained. Some of the chatter motion was attributed to the inexperience of the subject used for this sequence of measurements. Subsequentially the movie data for the leg position measurement, listed in Appendix A, are illustrated in Figure 38. The abscissa is plotted in terms of movie frames and time. The timing was obtained from the light pulses on the film and

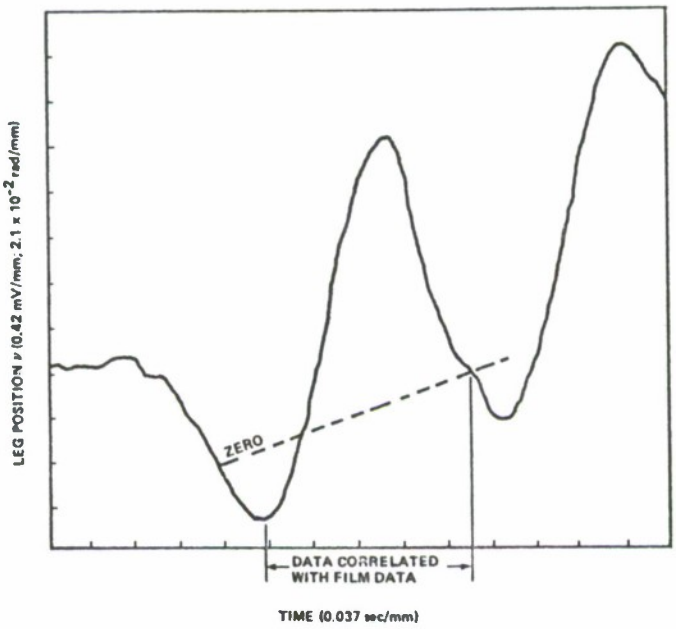

Figure 37. Position of leg (ν) with time

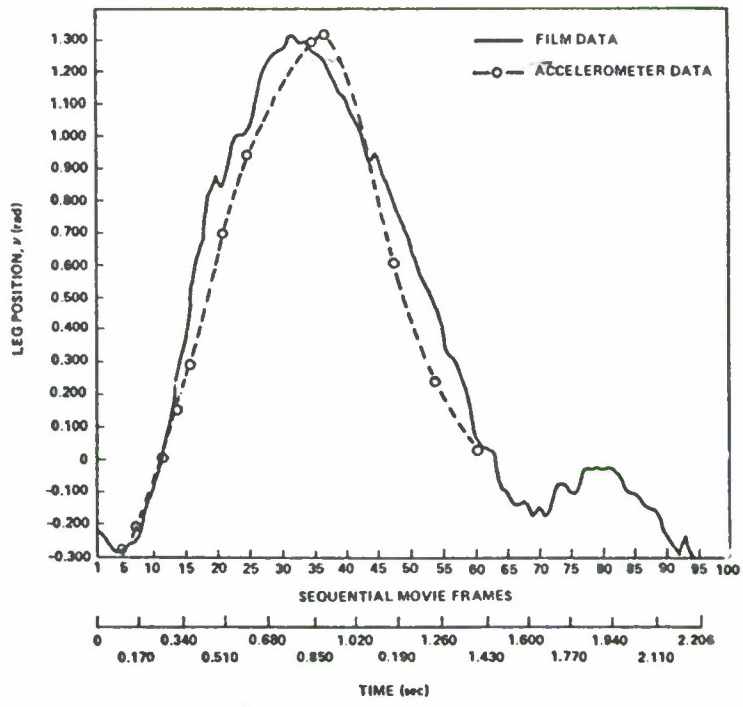

Figure 38. Leg link position data

enabled correlation of the recorded accelerometer data by pulses occurring on the strip chart recording (Figure 36, channel 4).

The maximum difference in position (θ) from the unsmoothed film data occurs 1.19 seconds from t_o. Although no acceleration data are available from the movie film for comparison, the average accelerometer acceleration indication occurs at t_o = 1.19 seconds and is approximately 5 rad/sec^2 in amplitude. The rate signal from the accelerometer shows a better reproduction of the film position than does the accelerometer data. This may be attributed to the smoothing incurred through the integration.

Figure 39 illustrates the accelerometer data obtained from the arm link of the system. Again the high frequency components of acceleration are present but the average acceleration amplitudes are lower than those observed for the leg link. Approximately 79.5 rad/sec^2 peak accelerations occurred in the arm motion. Also, the smoothing is evident in the position data when comparing the integrated position (Figure 40) and the movie position (Figure 41). The maximum difference in the arm position from film measurements occurs at -0.525 rad and is 21 percent in amplitude.

Due to the inability to correlate the position between the two data sources because of missing strobe pulses on the film, a subsequent test was conducted with strobe pulse having a 25-msec pulse width and a 200-msec period. Further testing of the 16-mm camera employed in this sequence of tests revealed an inherent speed instability. This was later verified by missing pulse occurrence with the wider strobe pulse.

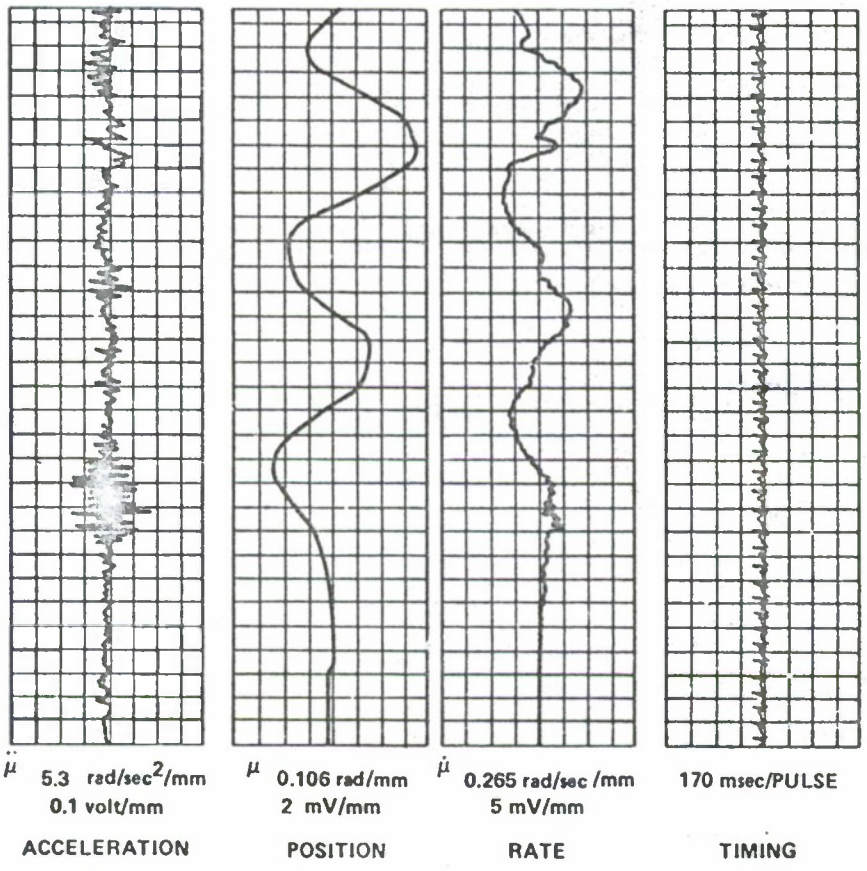

Figure 39. Arm link accelerometer data (after processing)

However, time correlation was much better in subsequent tests as illustrated in Figures 42, 43, and 44. Figure 42 presents the scaled raw data and subsequent computer manipulations. Figure 43 is merely an expanded plot of the position data (μ) obtained from the computer. Figure 44 presents a composite illustration of the pictorial position data and the accelerometer position data. In view of the uncertainty in the frame rate for the pictorial data, a worse case position error was assumed at the occurrence of a timing pulse and a strobe pulse that could be definitely identified. This worst case difference occurred

at 0.75 sec (Figure 44) and resulted in a percent difference of

$$\frac{0.011 \text{ rad}}{0.203} \times 100 = 5.4 \text{ percent}$$

The accelerometer data for this calculation were obtained from Figure 42.

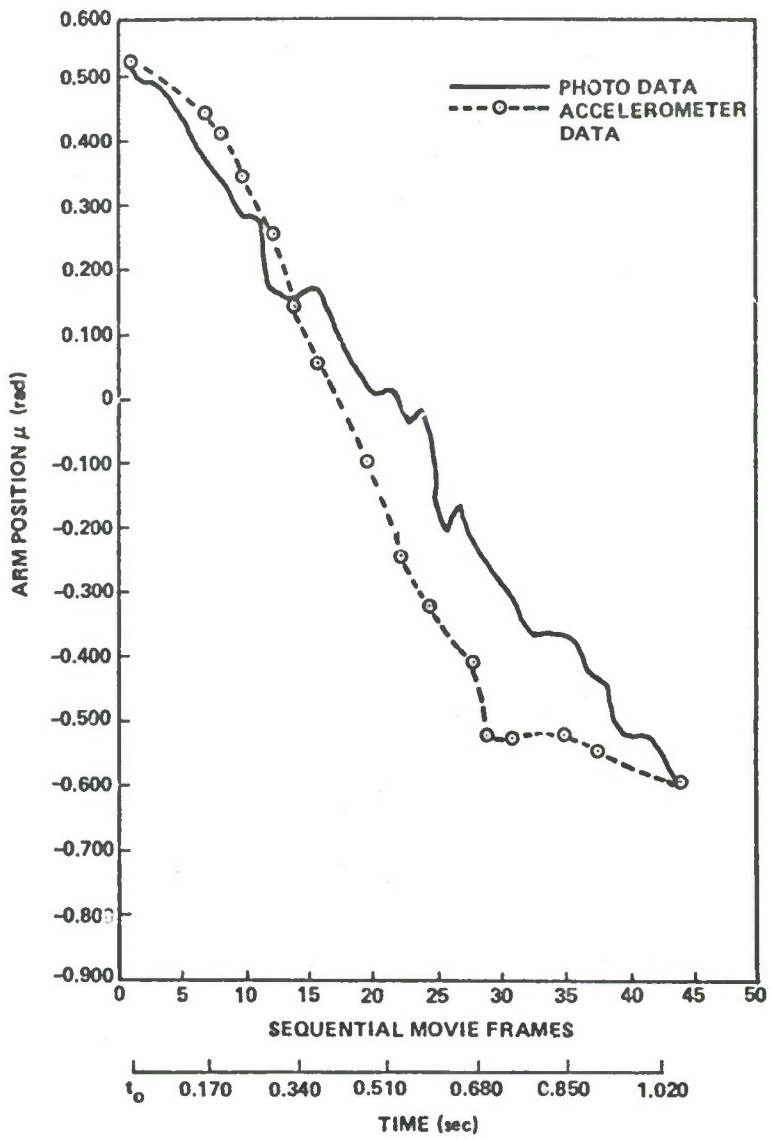

Figure 40. Arm link position (μ) data

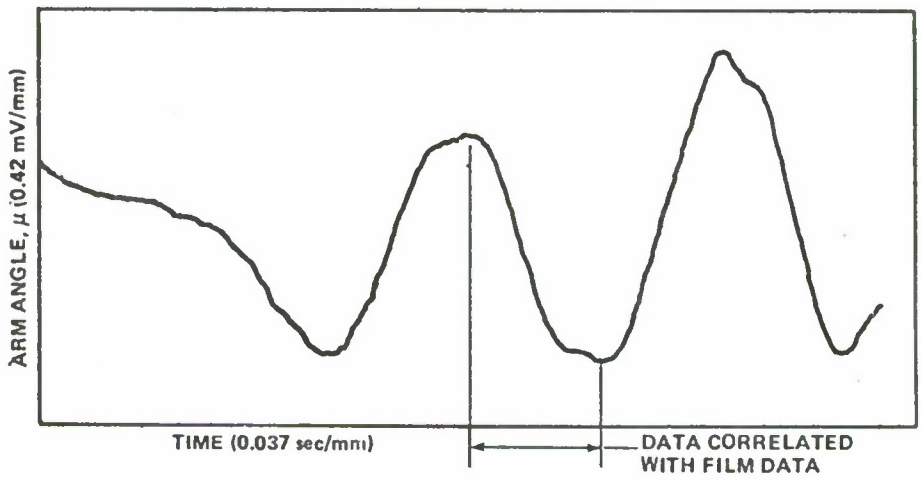

Figure 41. Position of arm (μ) as a function of time

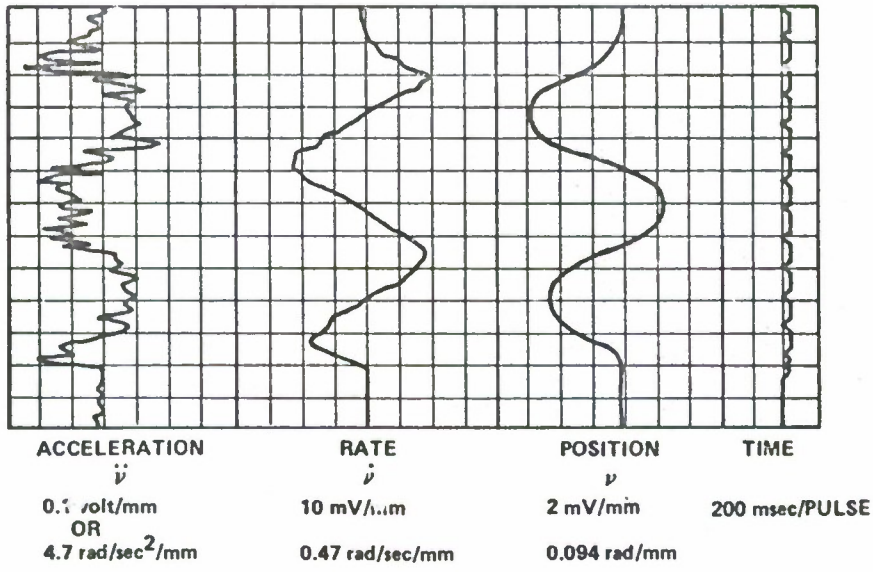

Figure 42. Accelerometer data of arm (μ) off high bar

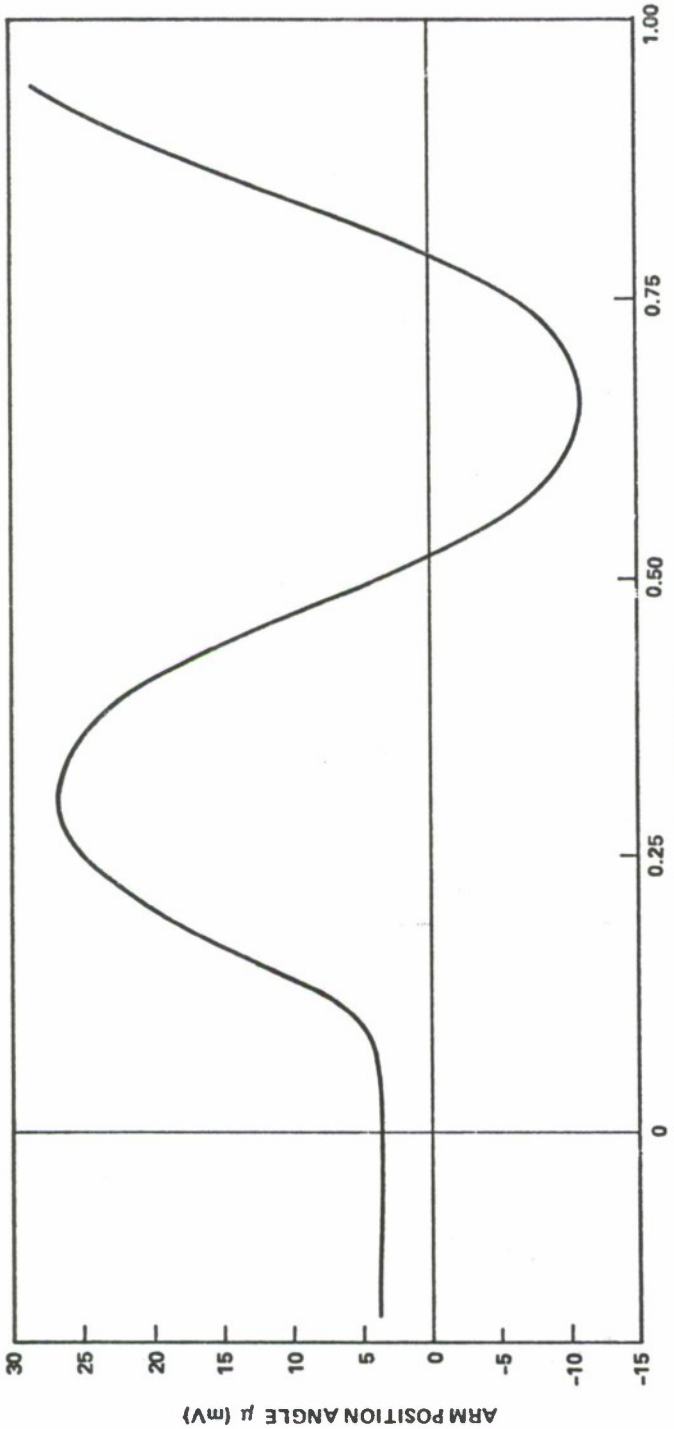

Figure 43. Expanded arm position angle (μ)

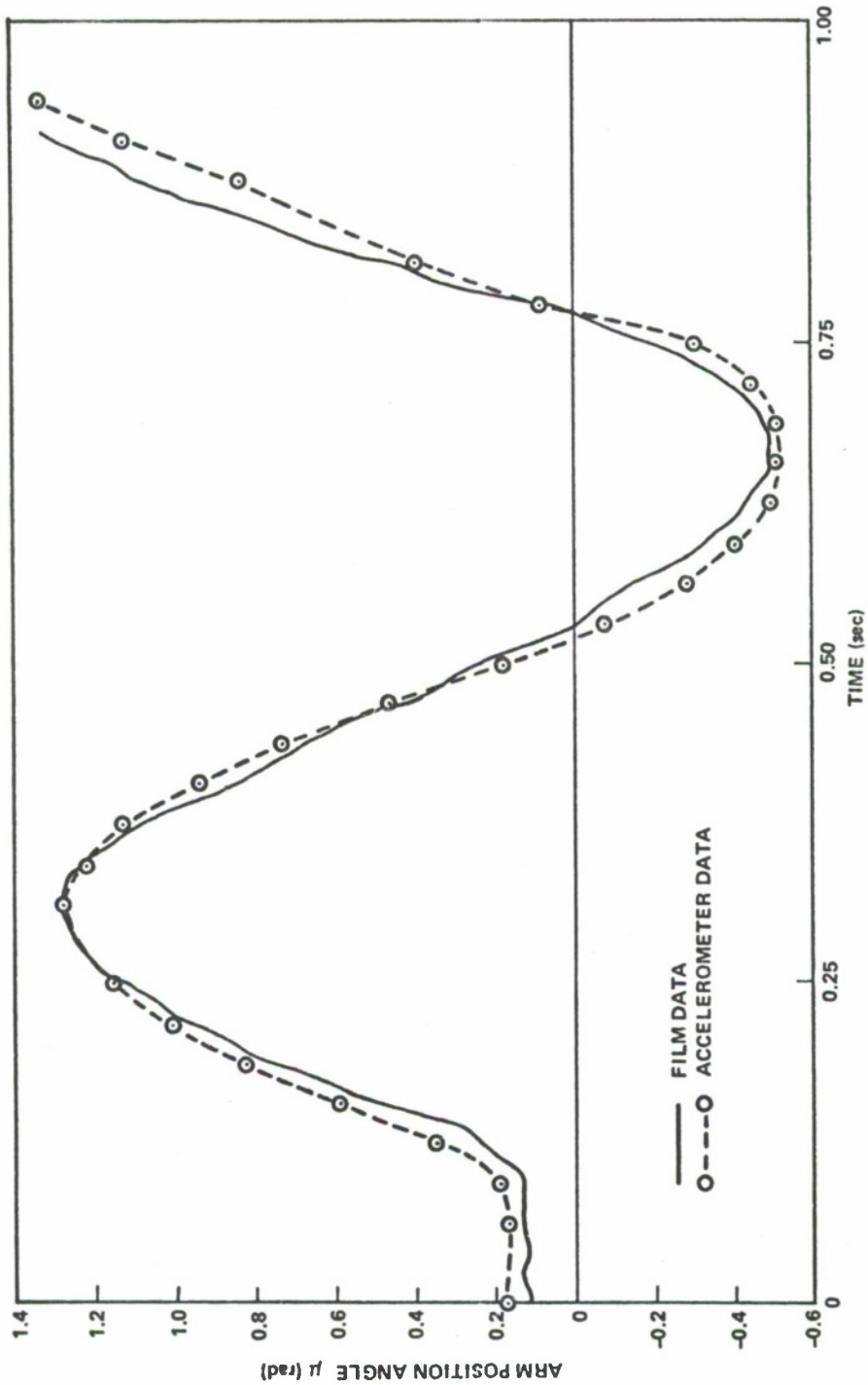

Figure 44. Composite film and accelerometer position angle (μ)

CHAPTER IV. SUMMARY AND CONCLUSIONS

Summary

The three sets of data collected and analyzed revealed inaccuracies in the timing of the reference pictorial data. In using the mechanization of the timing correlation technique, it was found that frame rates for the movie camera varied approximately 13 to 18 msec per frame which could produce on error in timing by a factor of:

$$\frac{5 \text{ msec}}{17 \text{ msec}} \times 100 = 29 \text{ percent}$$

Thus by viewing Figure 44 it is apparent that position discrepancies are the result of timing rather than amplitude.

In comparing the position angle (ν) between the film and that obtained from the accelerometer, there exists a 5.4-percent difference maximum. Some of this difference is due to problems associated with extracting the position angle from the film and correlation of these data with respect to time. It can be concluded that even the angle obtained from the acceleration data could be the more accurate of the two values. Certainly, acceleration and rate data from the accelerometer should be much more accurate than that derived from film.

Conclusions

Many obstacles were encountered during the experiments conducted for this thesis. Due to these obstacles, many recommendations are appropriate. The foremost problem encountered was the stray RF radiation in the telemetry package.

The telemetry package should be reconfigured to enable use of the circuit housing as an RF shield. Problems encountered with RF entering the analog to frequency conversion circuitry can be reduced significantly by proper circuit layout and RF shielding. Also, in the area of RF shielding, leads for the EMG sensors must be shielded completely. Complete shielding of the leads means using cable connections to interface the telemetry package with the shielded EMG leads. In conjunction with these recommendations, provisions should be made to allow a greater distance between the telemetry receiver site and the transmitter site when conducting future tests. The RF energy radiated by the telemetry transmitter over drives the RF section of the receiver when the two elements are operated in the same room.

Provisions to enable recharging the battery power supply should be considered. In the redesign of the telemetry package, a connector should be included that will allow a simple, quick interface between the battery charging source and the batteries. Also, a two-position switch should be provided that completes the charging circuit only in one position and enables operation of the telemetry package in the second position.

During the data analysis, transients of at most 150 rad/sec^2 were observed although average accelerations were much less. Therefore, an

accelerometer with a dynamic range of no more than 200 rad/sec^2 should be employed in future experiments.

The accelerometer alignment techniques employed proved to be accurate. However, it is recommended that a form fitted surface interface the subjects leg and the accelerometer gimbal assembly. A more positive contact is needed between the subjects leg and the gimbal assembly than can be accomplished with a foam rubber padding that compresses into the proper shape.

Data storage provided a challenge because of the limited quality of the recording equipment available. Also, data reduction on an analog computer is not a suitable approach to obtain rate and position data from the acceleration data. Future experiments should employ the tape recorder as the data storage element but provisions should be made to enable recording the raw data at a fast tape speed and then reducing the data at a slower tape speed. The speed variation will in essence introduce a time scaling such that the data can be effectively and accurately digitized for analysis on the digital computer. Use of the digital computer to analyze the data permits eliminating with software in the computer any dc offsets, which are extraneous values. In contrast, the sequential integrations performed on the analog computer cannot effectively handle dc offsets or variable initial conditions.

Implementation of the recommended modifications and procedures associated with the system evaluated in this thesis would enable realizing a system far superior to the technique of extracting body motion data from movie film. In conclusion, this body motion measurement system is quite suitable for monitoring body motion in an

environment where the shock levels are low and the motions are relatively smooth and have perturbations with frequency components less than 60 Hz.

APPENDIX A. MOTION PICTURE AND TELEMETRY DATA

Table A-I. Leg mount angles

Frame No.	Angle, ν		Frame No.	Angle, ν	
	deg	rad		deg	rad
1	- 11.5	- 0.201	20	49.9	0.871
2	- 12.8	- 0.224	21	48.0	0.838
3	- 14.8	- 0.258	22	52.1	0.909
4	- 16.5	- 0.288	23	58.5	1.002
5	- 16.7	- 0.292	24	59.4	1.004
6	- 15.0	- 0.262	25	61.8	1.008
7	- 15.0	- 0.262	26	65.2	1.104
8	- 12.8	- 0.224	27	68.4	1.195
9	- 9.0	- 0.157	28	70.3	1.228
10	- 5.8	- 0.101	29	71.7	1.253
11	- 2.0	- 0.035	30	72.0	1.260
12	2.3	- 0.040	31	74.7	1.305
13	6.4	0.112	32	74.7	1.305
14	16.0	0.280	33	73.5	1.283
15	19.9	0.348	34	73.8	1.290
16	29.2	0.510	35	72.2	1.260
17	34.6	0.605	36	71.8	1.253
18	40.0	0.700	37	71.0	1.240
19	46.5	0.812	38	68.3	1.192

Table A-I. Continued

Frame No.	Angle, ν deg	Angle, ν rad	Frame No.	Angle, ν deg	Angle, ν rad
39	65.1	1.137	63	1.9	0.024
40	64.6	1.128	64	- 5.1	- 0.089
41	60.9	1.063	65	- 5.2	- 0.091
42	59.2	1.032	66	- 7.9	- 0.138
43	57.3	1.000	67	- 7.8	- 0.136
44	53.0	0.925	68	- 7.0	- 0.122
45	54.3	0.947	69	- 10.1	- 0.177
46	50.0	0.874	70	- 8.2	- 0.143
47	48.2	0.843	71	- 9.8	- 0.171
48	43.9	0.766	72	- 8.0	- 0.140
49	41.8	0.730	73	- 4.7	- 0.082
50	39.4	0.689	74	- 4.3	- 0.075
51	35.2	0.615	75	- 5.4	- 0.094
52	31.8	0.556	76	- 6.1	- 0.107
53	30.0	0.524	77	- 2.0	- 0.035
54	26.7	0.466	78	- 1.9	- 0.032
55	23.1	0.404	79	- 1.3	- 0.023
56	19.0	0.332	80	- 2.0	- 0.035
57	18.0	0.314	81	- 1.3	- 0.023
58	14.7	0.257	82	- 2.0	- 0.035
59	10.4	0.184	83	- 3.9	- 0.058
60	4.5	0.079	84	- 5.7	- 0.099
61	2.0	0.035	85	- 6.0	- 0.105
62	1.8	0.031	86	- 6.9	- 0.121

Table A-I. Concluded

Frame No.	Angle, ν deg	Angle, ν rad	Frame No.	Angle, ν deg	Angle, ν rad
87	- 8.5	- 0.149	91	- 15.0	- 0.262
88	- 8.8	- 0.154	92	- 16.9	- 0.294
89	- 10.0	- 0.175	93	- 13.6	- 0.238
90	- 13.4	- 0.234	94	- 17.0	- 0.297

Table A-II. Arm mount angles on bar

Frame No.	Angle, ϕ deg	Angle, ϕ rad	Frame No.	Angle, ϕ deg	Angle, ϕ rad
1	30.2	0.525	17	7.5	0.131
2	28.0	0.488	18	4.8	0.084
3	28.0	0.488	19	2.8	0.049
4	27.0	0.472	20	0.5	0.009
5	25.6	0.447	21	0.6	0.010
6	23.0	0.402	22	1.0	0.017
7	21.4	0.374	23	- 2.0	- 0.035
8	20.0	0.350	24	- 6.0	- 0.015
9	18.0	0.314	25	- 8.8	- 0.154
10	15.8	0.276	26	- 11.8	- 0.206
11	16.2	0.283	27	- 9.3	- 0.162
12	10.0	0.175	28	- 12.8	- 0.224
13	9.6	0.168	29	- 14.5	- 0.253
14	9.0	0.157	30	- 16.3	- 0.284
15	9.6	0.168	31	- 17.7	- 0.309
16	9.8	0.171	32	- 20.3	- 0.354

Table A-II. Concluded

Frame No.	Angle, ϕ deg	Angle, ϕ rad	Frame No.	Angle, ϕ deg	Angle, ϕ rad
33	- 21.0	- 0.366	39	- 29.2	- 0.510
34	- 21.0	- 0.366	40	- 30.0	- 0.524
35	- 21.0	- 0.366	41	- 29.8	- 0.520
36	- 21.7	- 0.379	42	- 30.4	- 0.532
37	- 24.3	- 0.425	43	- 32.8	- 0.574
38	- 25.0	- 0.437	44	- 34.8	- 0.608

Table A-III. Arm position (μ) data off high bar

Frame No.	Strobe Pulse	Angle deg	Angle rad	Frame No.	Strobe Pulse	Angle deg	Angle rad
0		6.5	0.114	14		36.0	0.628
1		7.0	0.122	15		41.5	0.725
2		7.8	0.136	16		48.0	0.840
3		6.6	0.115	17		51.7	0.904
4		6.9	0.121	18	1	57.1	0.996
5		7.5	0.131	19		60.5	1.060
6		7.4	0.129	20		64.0	1.118
7		7.4	0.129	21		68.4	1.194
8		7.7	0.135	22		70.0	1.223
9		11.3	0.198	23		71.8	1.255
10		13.2	0.231	24		73.1	1.277
11		16.4	0.286	25		73.4	1.282
12		24.5	0.428	26		73.3	1.278
13		29.8	0.522	27		72.0	1.258

Table A-III. Concluded

Frame No.	Strobe Pulse	Angle deg	Angle rad	Frame No.	Strobe Pulse	Angle deg	Angle rad
28		69.6	1.217	49		- 28.0	- 0.489
29		66.6	1.163	50		- 29.0	- 0.507
30		63.0	1.100	51		- 27.7	- 0.484
31		58.5	1.021	52		- 26.4	- 0.462
32		53.1	0.926	53		- 24.5	- 0.427
33	2	48.0	0.838	54		- 20.5	- 0.358
34		42.3	0.737	55		- 17.0	- 0.297
35		35.8	0.625	56	3	- 11.6	- 0.203
36		28.4	0.496	57		- 4.8	- 0.084
37		18.3	0.320	58		1.0	0.017
38		14.5	0.253	59		10.3	0.180
39		5.0	0.087	60		20.0	0.349
40		- 2.8	- 0.049	61		25.6	0.447
41		- 6.2	- 0.108	62		35.0	0.611
42		- 12.5	- 0.218	63		42.0	0.733
43		- 16.7	- 0.292	64		47.5	0.829
44		- 19.5	- 0.341	65		56.0	0.978
45		- 23.0	- 0.402	66		62.5	1.092
46		- 25.0	- 0.437	67		65.0	1.137
47		- 26.5	- 0.463	68		71.0	1.240
48		- 28.0	- 0.489	69		75.7	1.322
				70		79.2	1.383

APPENDIX B. ACCELEROMETER DATA

Angular Accelerometer
Model 4591F-200-A
Serial No. 197

Range	200	rad/sec^2
Calibration (Voltage Scale Factor)	0.0204	$volt/rad/sec^2$
Output Impedance	1.2	Kohms
Output Noise	2.5	mV rms
Output for "0" Rad Input (Zero Output Null)	0.0002	Vdc
Natural Frequency (90° Phase Shift)	111	cps
Damping Ratio	0.69	
Hysteresis	< 0.05	percent full range
Nonrepeatability	< 0.02	percent full range
Temperature Coefficient of Voltage Scale Factor	0.0242	percent/°F
Temperature Coefficient of Zero Output	0.00625	mV/°F
Linear Accelerometer Sensitivity	0.9	mV/g

Temperature Range 0 to 160°F

S-D Outline Drawing No. 24054

NOTE: For normal operation jumper pins 1 and 2

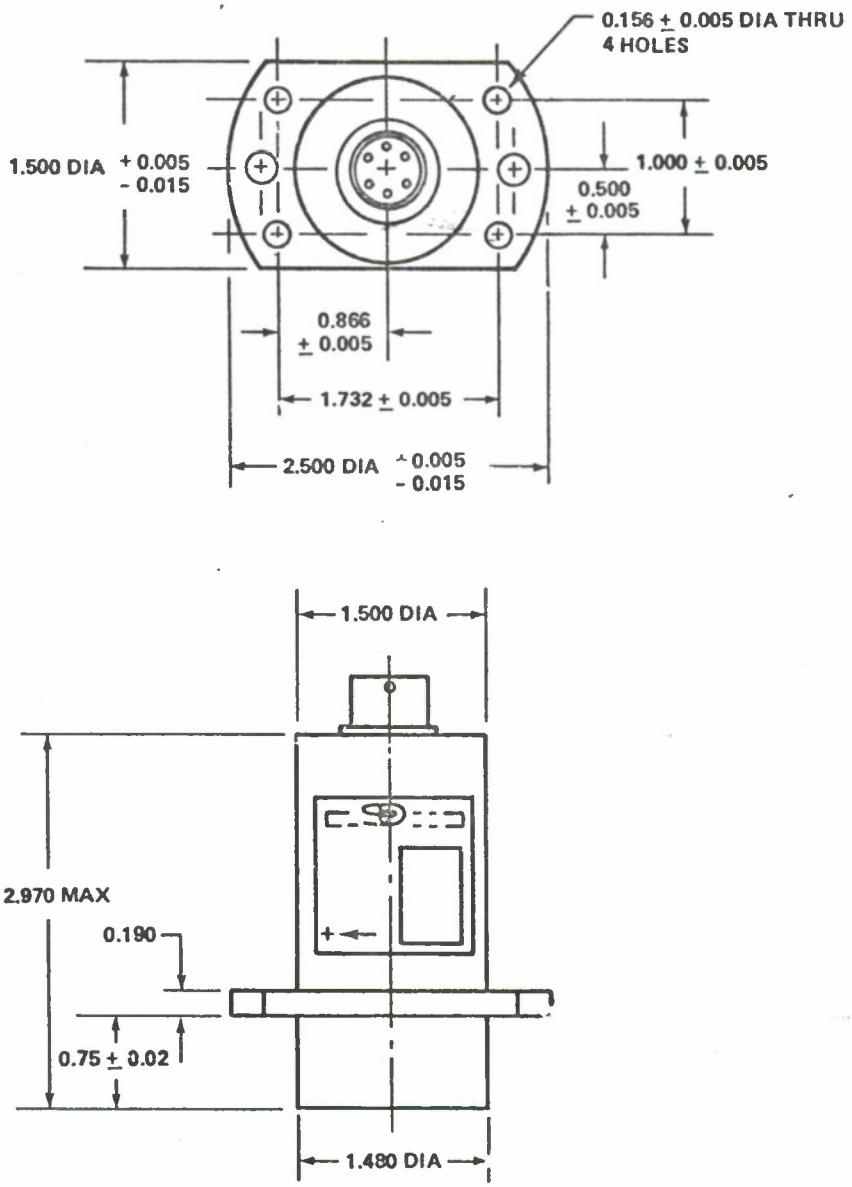

Figure B-1. Accelerometer outline and dimension diagram

APPENDIX C. TELEMETRY SYSTEM

The FM transmitter output power is approximately 200 mW and operates at 231.9 MHz (Figure C-1). The power requirements are approximately 100 mA at 28 Vdc. No calibration is required for the transmitter before operation. A quarter wave stub antenna, approximately 31.2 cm long, is adequate for all operations.

The mixer amplifier power requirements are 10 mA at 28 Vdc. The output amplitude should be approximately 2 volts peak-to-peak which produces the 60-percent modulation of the transmitter. The output amplitude is adjustable at the top of the module along side the output monitoring jack.

The variable frequency oscillator has the same power requirements as the mixer amplifier. However, the VCO has three adjustments and a test point on top of the module. The adjustments are:

F Center frequency adjust

S Scaling or voltage sensitivity adjust

L Output amplitude adjust (should be approximately 2.5 volts peak-to-peak).

The VCO's employed here are proportional bandwidth and follow IRIG telemetry standards. Table C-I describes the channels that may be used with this system along with the respective discriminator.

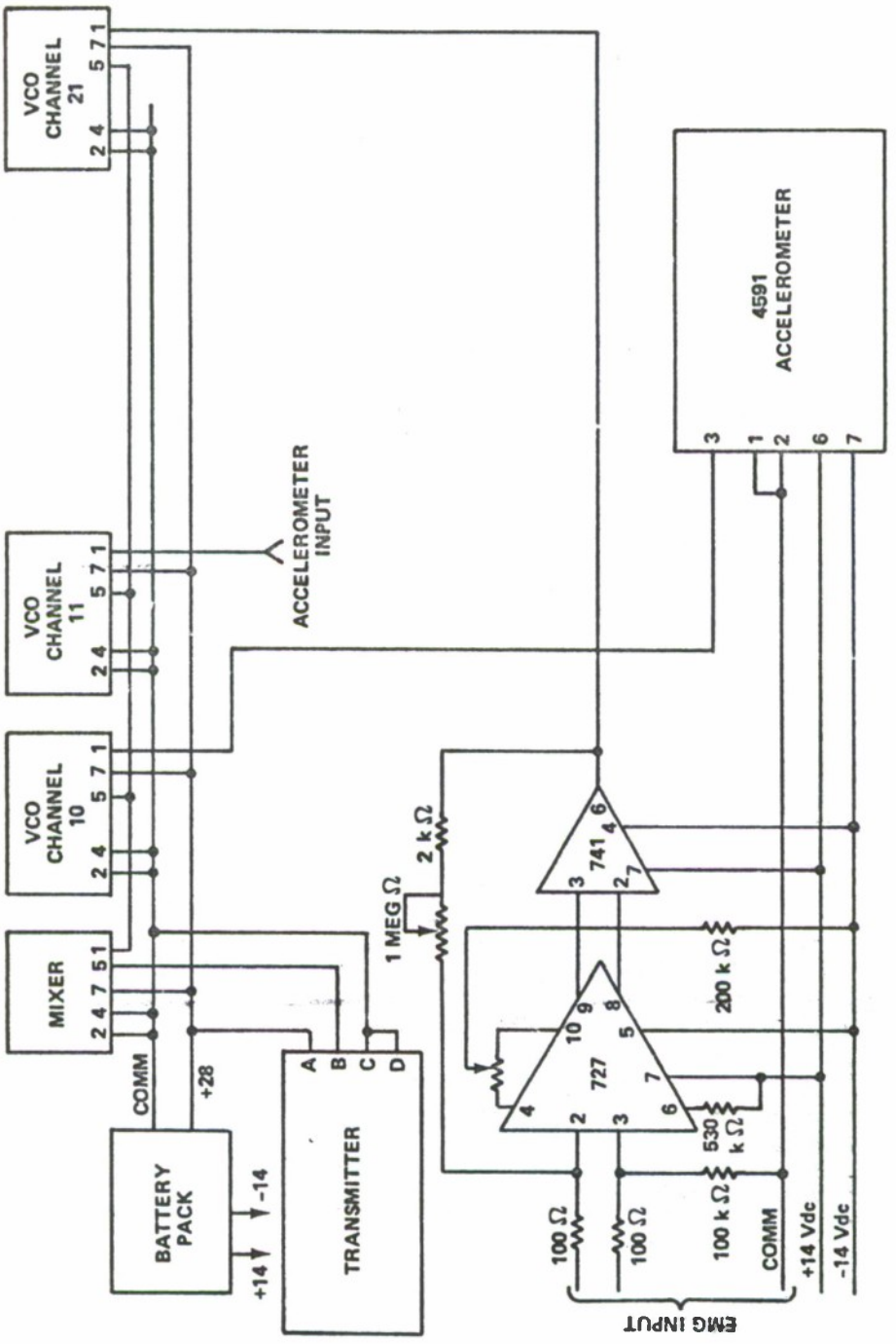

Figure C-1. Telemetry schematic diagram

Table C-I. Variable frequency oscillator channel allocation

Channel No.	Center Frequency (kHz)	Deviation (%)	Maximum Duty Cycles
1	0.40	7.5	6.0
2	0.56	7.5	8.4
3	0.73	7.5	11.0
4	0.96	7.5	14.0
5	1.3	7.5	20.0
6	1.7	7.5	25.0
7	2.3	7.5	35.0
8	3.0	7.5	45.0
9	3.9	7.5	59.0
10	5.4	7.5	81.0
11	7.35	7.5	110.0
12	10.5	7.5	160.0
13	14.5	7.5	220.0
14	22.0	7.5	330.0
15	30.0	7.5	450.0
16	40.0	7.5	600.0
17	52.5	7.5	790.0
18	70.0	7.5	1050.0
19	93.0	7.5	1390.0
20	124.0	7.5	1860.0
21	165.0	7.5	2470.0

Calibration of the VCO's requires a precision E-put counter capable of 0.01 Hz resolution at a frequency of 165 kHz and an

oscilloscope. The VOC center frequency is set by grounding the input to the VCO at pin number 1 and observing the counter for the proper frequency of a given module when connected to the output test point. The scale factor calibration requires a ±2.5-volt input at pin 1 while observing a ±7.5-percent deviation of the center frequency of the VCO. (Figure C-2). Adjust trim pot L to obtain the required deviation. Again, short the input to the VCO and connect an oscilloscope to the output test point and adjust trim pot S for a 2.5-volt peak-to-peak output.

VCO CALIBRATION CIRCUIT

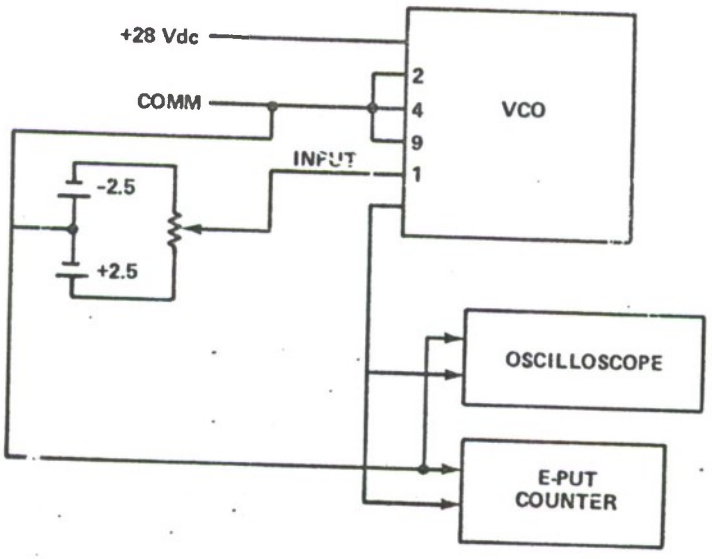

Figure C-2. VCO calibration circuit

Manuals are available for the receiving equipment, hence they should be referred to in regard to the pertinent equipment.

Parts List

Transmitter:	P/N CTM-402, Conic Corporation
Mixer Amplifier:	P/N CMA-400A; IED Division of Conics Corporation
VCO:	P/N CSO-220-1; ±2.5 volts; IED Division
Accelerometer:	Model 4591-200A; Systron-Donner
Preamplifier	U5U7727333; Fairchild
Op-amp:	FU5B 7741393 7114; Fairchild
Trim Pots:	1 Megohm, 78PR1 Meg; Helitrim 250 K ohm, 78PR250K; Helitrim

REFERENCES

1. Geneesk, N. T. V., "Uber die Veranderung der Kraft Wahrend der Bemegung," Archiv fur die Gesamte Physiologie, Volume 191: 234-257, 1921.

2. Eshkol, N., Notion of Movement, Final Report, 1 March, 1968, to 31 August, 1969; Grant DA-ARO-D-31-124-6998, U.S. Army, 15 February, 1970. Department of Electrical Engineering, University of Illinois.

3. Calvity, Harry H. and Rosenthal, Arnold, Analysis of the Structural Dynamics of the Human Body, Department of the Army Project No. DA36-034-AMC0207R, Department of Engineering Mechanics Report, Pennsylvania State University, 1967.

4. Ramsey, J. D., The Quantification of Human Effort and Motion for The Upper Limbs, Department of the Army Project No. DAAD05-69-C-0102, Department of Industrial Engineering, Texas Technological College, February, 1968.

5. Ramsey, J. D., Ayoub, M. A., Ayoub, M. M., System for Measuring Human Motion, Department of the Army Project No. DAAD05-69-C-0102, Department of Industrial Engineering, Texas Technological University, 1970.

6. Edwards, E., "Research Note on the Study of Hand Motions," Perceptual and Motor Skills, Volume 20, June 19, 1965, Part 2, p. 1098.

7. Hixson, W. C., Beischer, D. E., Biotelemetry of the Ballisto-cardiogram and Electrocardiogram in a Weightless Environment, U.S. Naval School of Aviation Medicine, Pensacola, Florida, 8 September, 1964.

8. Samras, R. K., Muscle Torque Measurement, Effects on Optimal Motion, and Human Performance Evaluation, University of Florida, Masters Thesis, Department of Engineering Science and Mechanics, 1971.

END

FILMED

12-18-72

NTIS